Materials Today Bio 23 (2023) 100813

Contents lists available at ScienceDirect

Materials Today Bio

journal homepage: www.journals.elsevier.com/materials-today-bio

Injectable hyperbranched PEG crosslinked hyaluronan hydrogel microparticles containing mir-99a-3p modified subcutaneous ADSCs-derived exosomes was beneficial for long-term treatment of osteoarthritis

Zhaowei Yin [a], Chaoren Qin [c], Shaowei Pan [a], Chen Shi [a], Guanfu Wu [b], Yan Feng [c], Jing Zhang [b], Ziyi Yu [b], Bin Liang [a], Jianchao Gui [c,*]

[a] Department of Orthopaedics, Nanjing First Hospital, Nanjing Medical University, Nanjing 210006, China
[b] State Key Laboratory of Materials-Oriented Chemical Engineering, College of Chemical Engineering, Nanjing Tech University, 30 Puzhu South Road, Nanjing 211816, PR China
[c] Sports Medicine and Joint Surgery, Nanjing First Hospital, Nanjing Medical University, Nanjing 210006, China

ARTICLE INFO

Keywords:
Osteoarthritis
Mesenchymal stem cells
Exosomes
MicroRNA
Microfluidics
Hydrogel

ABSTRACT

Exosomes (Exos) secreted by adipose-derived stem cells (ADSCs) have shown potential in alleviating osteoarthritis (OA). Previous studies indicated that infrapatellar fat pad (IPFP) derived stem cells (IPFSCs) may be more suitable for the treatment of OA than subcutaneous adipose tissue (ScAT) derived stem cells (ScASCs). However, it remains unclear which type of Exos offers superior therapeutic benefit for OA. This study first compared the differences between Exos derived from IPFP stem cells ($Exos^{IPFP}$) and ScAT stem cells ($Exos^{ScAT}$) in OA treatment. Results suggested that $Exos^{IPFP}$ significantly inhibit the degradation of cartilage extracellular matrix (ECM) than $Exos^{ScAT}$, following this, the differences in microRNA (miRNA) expression between the two types of Exos using small RNA sequencing were performed. Subsequently, miR-99 b-3p was chosen and over-expressed in $Exos^{ScAT}$ ($Exos^{ScAT-99b-3p}$), both in vivo and in vitro experiments demonstrated its efficacy in inhibiting the expression of ADAMTS4, promoting the repair of the ECM in OA. Finally, microfluidic technology was performed to fabricate a hyaluronan-based hydrogel microparticles (HMPs) for encapsulating Exos (HMPs@exos), the injectability, sustained release of Exos and long-term therapeutic effect on OA were validated. In summary, these results suggest miR-99 b-3p regulates the degradation of cartilage ECM by targeting ADAMTS4, the upregulation of miR-99 b-3p in $Exos^{ScAT}$ would enable them to exhibit comparable or even superior effectiveness to $Exos^{IPFP}$ for OA treatment, making it a promising approach for OA treatment. Considering the abundant resources of ScAT and the limited availability of IPFP, ScAT harvested through liposuction could be genetically engineered to yield Exos for OA treatment. Furthermore, the encapsulation of Exos in HMPs provides an injectable sustained local drug release system, which could potentially enhance the efficacy of Exos and hold potential as future therapeutic strategies.

1. Introduction

OA is a slowly progressive and degenerative disorder that induces irreversible pathological changes such as damage to articular cartilage, remodeling of subchondral bone, inflammation of the synovial membrane, degeneration of ligaments and changes in muscles [1]. Numerous factors contribute to the development of OA, such as body weight, diet, age, and history of trauma [2]. The gradual loss of chondrocytes is the major cause of OA since chondrocytes are critical for the formation and maintenance of articular cartilage [3]. OA is characterized by the loss of ECM and cartilage destruction [4,5] Promoting articular cartilage repair or regeneration is the key to preventing OA progression. However, current treatments for OA are inadequate in terms of therapeutic effect.

Recently, mesenchymal stem cells (MSCs) isolated from human adipose tissue have been identified as an important source of multipotent adult stem cells, which have been widely used as an engineering stem cell source for tissue regeneration [6–8]. Adipose tissue is found in many parts of the human body, and the IPFP and ScAT are common tissues

* Corresponding author.
E-mail address: gui1997@126.com (J. Gui).

https://doi.org/10.1016/j.mtbio.2023.100813
Received 16 June 2023; Received in revised form 19 August 2023; Accepted 21 September 2023
Available online 28 September 2023

types for stem cell extraction. ADSCs have several advantages over other MSCs. Intra-articular injection of ADSCs improves the function and reduces pain and cartilage defects of the knee joint [9]. In addition, ADSCs can be more easily cultured and obtained in vastly greater quantities by less aggressive methods than other MSCs [10].

Histologically, ScAT is mainly regarded as an endocrine and metabolic pool and has a mesodermal origin that is similar to bone and cartilage [11]. Moreover, it secretes a number of bioactive substances that exhibit anti-inflammatory and immunomodulatory characteristics [12]. IPFP is a mass of fibrous adipose tissue, mainly composed of synovium and subsynovial adipose tissue [13]. IPFP has more blood vessels and nerves and is more similar to visceral fat than ScAT [14]. IPFP-derived stem cells (IPFSCs) exhibit unique properties in terms of proliferation capacity and multilineage differentiation potential [15]. Some studies suggest that the therapeutic effect of IPFSCs on OA is better than that of subcutaneous adipose-derived stem cells (ScASCs). Mochizuki et al. showed that IPFSCs have higher chondrogenic potential than ScASCs [13].

However, the transplantation of MSCs also has risks that may cause immune rejection and potential tumorigenicity [16]. An increasing amount of evidence supports that the mechanisms underlying the therapeutic effects are likely paracrine mechanisms of MSCs, particularly Exos secretion [17]. Since the first report, MSC Exos have replicated many of the wide-ranging therapeutic effects of MSCs in numerous animal models of injuries and diseases. However, it is unknown which kind of ADSCs-exos is more effective in the treatment of OA [16,18].

Exos are membranous vesicles with diameters ranging from 30 to 150 nm that move into the ECM after the integration of intracellular polyvesicles and cell membranes [19]. These vesicles can be secreted by many kinds of cells and have been reported to promote chondrocyte regeneration, inhibit apoptosis, and improve ECM balance, thus affecting the fate of cells or tissues [20–23]. Moreover, Exos contain many functional miRNAs, and miRNAs have the ability to modulate the expression of multiple genes implicated in various kinds of physiological functions and disease processes, such as OA. Previous studies have demonstrated that miRNAs play a key role in mediating the effects of the main risk factors for OA through the control of target genes and are critical in the pathological process of OA [23–26].

Clinically, the IPFP is often routinely removed and disposed of as surgical waste during arthroscopy or open knee surgery, and most of it comes from elderly patients (who usually also have chronic diseases) with knee arthroplasty [27,28]. Therefore, it has higher expression of inflammatory genes, releases more inflammatory factors, and contains more immune cells than ScAT [15,29]. ScAT can be easily obtained from patients in large volumes with minimal inflammation by liposuction [30]. Therefore, it is particularly important to explore the difference in the expression of miRNAs between the two ADSC-derived Exos types ($Exos^{ScAT}$ and $Exos^{IPFP}$). By regulating the expression of key miRNAs, the effect of $Exos^{ScAT}$ in OA treatment may be better than that of $Exos^{IPFP}$. In future clinical work, abundant resources of ScAT will allow large quantities of stem cell culture and Exos to be produced to obtain enough high-quality Exos to facilitate their use as effective biological agents for OA treatment.

Additionally, Exos have a short half-life in vivo, and injected Exos are easily cleared by the body's immune system, resulting in a short retention time and low bioavailability at the target site, which limits their therapeutic potential in the clinic. Hydrogels can be used as effective drug loading materials to control drug release in situ. Various kinds of hydrogels have been used to protect Exos and enhance the therapeutic effects of Exos [7,21,31]. Among these hydrogel materials, poly (ethylene glycol) (PEG) has been extensively used for the fabrication of biocompatible hydrogels for tissue engineering and cartilage repair [32,33]. Hyaluronic acid (HA) is one of the most versatile and fascinating macromolecules in the natural world and is one of the most widely used medical treatments for OA [34]. It can be modified with various functional moieties to form functional hydrogels.

However, due to the heterogeneous shape and large size of conventional hydrogels, high and uneven injection forces, which may cause damage to healthy tissue and discomfort to patients, are inevitable during the injection process [35]. Additionally, the fabrication process of traditional hydrogel materials often involves the use of toxic reagents (such as small molecular monomers, crosslinking agents, etc.) or harsh synthesis conditions (radiation, high temperature, etc.), posing potential hazards to the stability of Exos. In light of these challenges, the Michael addition method for hydrogel material fabrication presents an ideal choice, as it offers advantages over conventional hydrogels, including mild reaction conditions and absence of by-products. Inspired by this, we, along with other researchers, developed an injectable hybrid hydrogel through the Michael addition reaction of hyperbranched poly (ethylene glycol) diacrylate (HB-PEGDA) and thiolated hyaluronic acid (SH-HA). This hydrogel exhibits versatile properties, good biocompatibility, and ease of application [36]. Furthermore, by utilizing a microfluidic device, we fabricated HMPs with enhanced structural stability, uniform size, and excellent injectability [37]. In the knee joint, when hyaluronidase or H_2O_2 presence, the HA-based HMPs act as effective sustained-release carriers, gradually degrading and releasing their contents.

In this study, we demonstrated the great importance of exosomal miRNAs in targeting cartilage and promoting ECM synthesis in OA. Moreover, we demonstrated the importance of the sustained release and prolonged effect of Exos for the treatment of OA. As shown in Scheme 1 and Scheme 2, we first studied whether ADSC-exos derived from IPFP are more suitable for ameliorating OA than ADSC-exos derived from ScAT in vitro and in a DMM model. Then, we investigated the regulatory mechanism by which the two kinds of ADSC-exo inhibit chondrocyte degeneration in OA. Through small RNA sequencing and bioinformatic analysis, we found that miR-99 b-3p may alleviate the development of OA by suppressing the expression of ADAMTS4 and reducing the loss of ECM. $Exos^{ScAT-99b-3p}$ (upregulation of miR-99 b-3p in $Exos^{ScAT}$) exhibit superior effectiveness to $Exos^{IPFP}$ for OA treatment. Finally, to address the short half-life of Exos, we prepared HMPs via the Michael addition reaction between SH-HA and HB-PEGDA in a droplet-based microfluidic device for encapsulating Exos and $Exos^{ScAT-99b-3p}$. The HMPs@Exos sustained the release of Exos for local and long-term therapeutic effects in the knee joint. In the murine OA model, the injectable $HMPs@Exos^{ScAT-99b-3p}$ effectively alleviated OA progression by promoting ECM synthesis. Taken together, these results indicate that injectable HMPs containing $Exos^{ScAT-99b-3p}$ that progressively target the ECM can be used for long-term therapy in OA and have great potential for application in future clinical work.

2. Materials and methods

2.1. Isolation of mouse ADSCs

8-week-old C57/B6J mice were sacrificed by cervical dislocation under isofurane anaesthesia. Adipose tissue was harvested from the inguinal areas and infrapatellar fat pad used in all experiments. Mouse ADSCs (mADSCs) were isolated from each adipose tissue sample. Briefly, adipose tissue was washed with phosphate-buffered saline (PBS) (pH 7.4) and cut into 0.5–1.0 mm small fragments. The tissues were then transferred into 15-mL tubes. Type I collagenase (1.0 mg/mL was then added to the tube at an identical volume. The mixture was immediately agitated using a water bass shaker (150 rpm) at 37 °C for 30 min. The digested tissue was filtered through a 40-μm cell strainer and centrifuged at 200×*g* for 5 min. The supernatant was aspirated and the cell pellet was resuspended in erythrocyte lysis buffer (168 mM NH4Cl, 10 mM KHCO3, and 0.1 mM EDTA4Na; 10 mL) at 4 °C for 10 min. After erythrocyte lysis, 5 mL of medium was added, and the tube was centrifuged at 200×*g* for 5 min. The cell pellet was resuspended in medium and filtered through sterilized 100- and 40-μm cell strainers (Corning Inc., NY, USA). The mADSCs were cultured and used in the

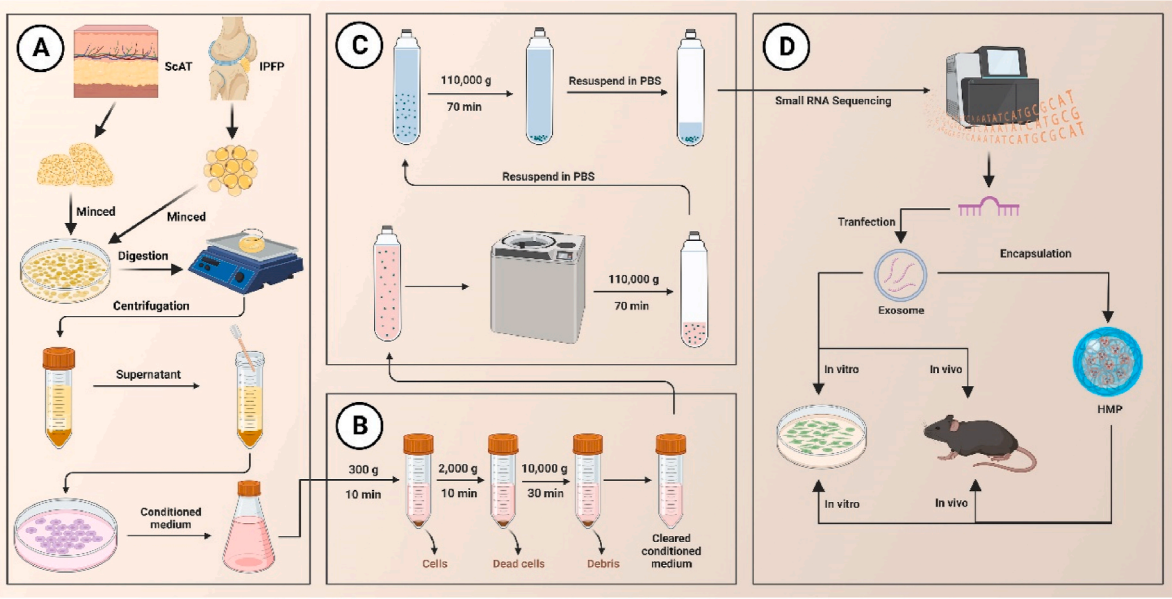

Scheme 1. Schematic illustration (Created with BioRender.com). (A) the process of isolating ADSCs from ScAT and IPFP. (B, C) the process of extracting Exos by using ultracentrifugation. (D) Small RNA sequencing was performed, and both in vitro and in vivo experiments were conducted. ScAT: subcutaneous fat; IPFP: infrapatellar fat pad.

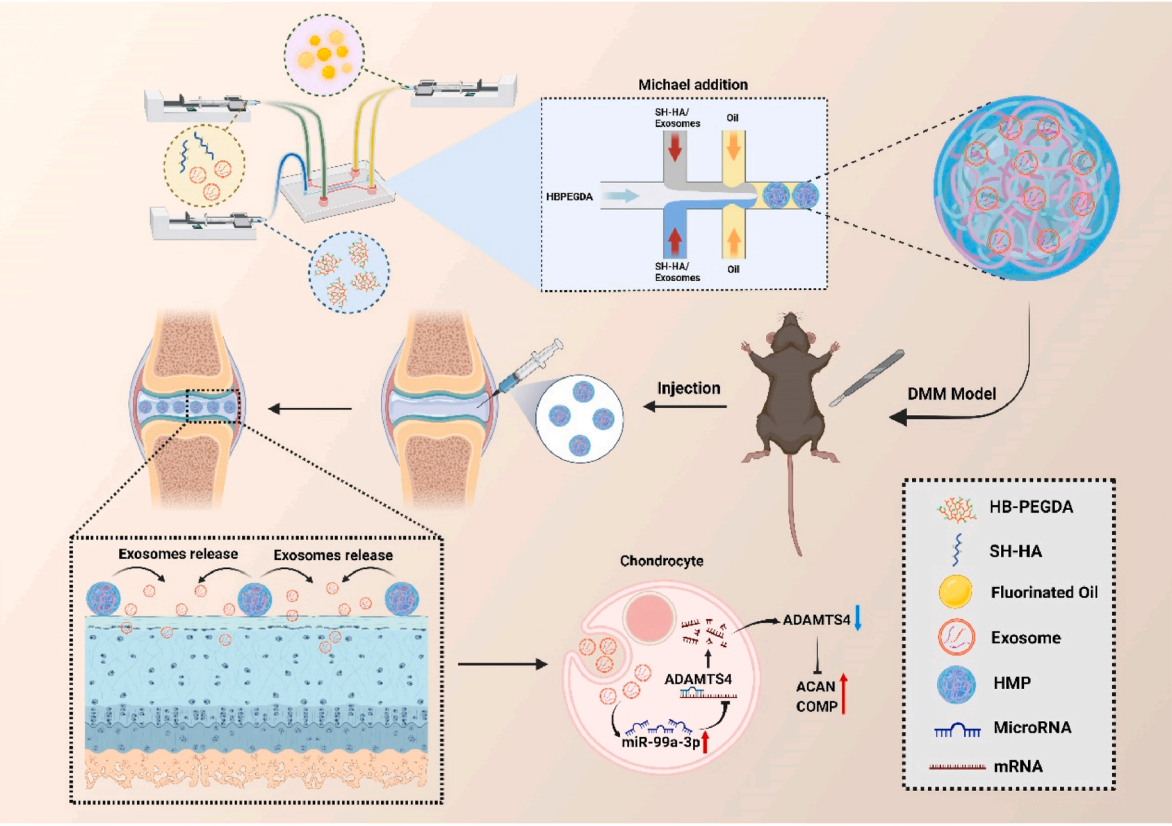

Scheme 2. Schematic illustration (Created with BioRender.com). Fabrication of HMPs and HMPs@Exos by microfluidics. Following intra-articular injection in a murine DMM model, the HMPs-Exos progressively degrade in the inflammatory environment, leading to gradually release of Exos. Exos are subsequently endocytosed by chondrocytes. ADAMTS4 expression is inhibited by over-expression of miR-99a-3b, promoting the repair of osteoarthritis. miR-99a-3p: microRNA-99 b-3p; ADAMTS4: ADAM Metallopeptidase with Thrombospondin Type 1 Motif 4; ACAN: aggrecan; COMP: cartilage Oligomeric Matrix Protein.

third passage.

2.2. Identification of ADSCs

For detecting the classical biomarkers of ADSCs, we performed flow cytometric analysis by the following fluorescein isothiocyanate- (FITC-) conjugated or phycoerythrin-(PE-) conjugated antibodies: CD29, CD44, CD90, CD105, CD73, CD34, and CD45 (Becton Dickinson, San Jose, CA, USA). The FITC-IgG and PE-IgG isotypic immunoglobulins were detected as isotype controls. After incubation, cells were washed twice and finally suspended in FACS buffer for flow cytometry analysis (BD Biosciences, USA).

The multipotent differentiation potential of ADSCs to differentiate to osteoblasts, adipocytes, and chondroblasts was evaluated. After subculturing to the third generation, the culture medium was replaced with osteogenic, adipogenic, or chondrogenic differentiation complete medium (Cyagen Biosciences, China). After the induction of the differentiation cultures for 14 days, the accumulation of calcium, intracellular lipids, and mucopolysaccharides was estimated by the alizarin red staining, oil red O staining, and Alcian blue staining (Sigma-Aldrich, USA), respectively.

2.3. Isolation of mouse-chondrocyte

To extract chondrocytes, 3-week-old C57/B6J mice were sacrificed for collection of cartilage from knees. First, cartilage was into small pieces after washing with PBS. Second, the samples were digested in 0.25% trypsin-EDTA (Gibco, USA) solution for 5 min, and DMEM-F12 (Gibco, USA) containing 0.2% collagenase type II (Sigma-Aldrich, USA) for 6 h at 37 °C, successively. The released chondrocytes were seeded in T25 cell culture flasks. Cells were passaged at a ratio of 1:3 at 80% confluence. The culture medium was refreshed every 3 days. Chondrocytes were induced with IL-1β (10 ng/mL) for 24 h after transfection for subsequent experiments.

2.4. Exos extraction and identification

The Exos derived from ADSCs were isolated as previously described. In brief, culture media supplemented with Exos-depleted FBS (SBI, USA) were used for cultivating ADSCs. Subsequently, conditioned supernatants from ADSCs cultures were collected and centrifuged such to remove dead cells or debris. The collected medium was subjected to ultracentrifugation at 110,000 g for 2 h at 4 °C after filtration with a 0.22-mm filter. The Exos-containing pellet was washed and resuspended with PBS and stored at −80 °C prior to further analysis. The total protein contents of the Exos were evaluated.

Analysis of particle size and intensity was conducted with nanoparticle trafficking analysis (NTA) system (NanoSight NS300). After isolation, the Exos were diluted infiltered PBS before administration. Samples were administered and recorded under controlled flow by the NanoSight syringe pump. Automatic settings were performed to measure the minimum particle size and track length. The measuring conditions were temperature 23.75 ± 0.5 °C, 25 frames per second, and measuring time 60s. The detection threshold was uniform in the different groups.

For morphologic observation with transmission electron microscopy (TEM), Exos pellets were seeded on formvar carbon-coated 200-mesh copper electron microscopy grids, placed at room temperature for 5 min, and then were stained with aqueous uranyl acetate. The grids were washed with PBS and continued to semidry at room temperature prior to detection under TEM (Hitachi, H7500 TEM, Tokyo, Japan).

The CD63, CD9, TSG101 and Calnexin biomarkers were measured with western blotting analysis. Exos were collected and resolved by SDS/PAGE and then transferred to PVDF membranes (Millipore, Billerica, MA, USA). The membranes were blocked by 5% nonfat milk in TBST buffer and incubated overnight using rabbit anti-CD63 (1:300, Proteintech, China), CD9 (1:1000, Proteintech, China), TSG101 (1:2000, Proteintech, China), Calnexin (1:5000, Proteintech, China) separately, then washed with TBST, and incubated continuously using HRP linked goat anti-rabbit IgG (1:5000, keen, China), and the protein intensity was determined with the automatic imager (General Electric, Fairfield, CT, USA).

2.5. Exos label and track

To determine whether ADSCs-exos can be taken up by chondrocytes, Exos were labelled with PKH26 (Sigma-Aldrich, USA) following the protocol recommended by the manufacturer. Which allow us to fluorescently label isolated Exos to track cellular interaction and uptake. Exos were co-cultured with chondrocytes then fixed with 4% paraformaldehyde. The nuclei were stained with Hoechst 33,342 (Beyotime, China). The cytoskeleton was stained by Actin-Tracker Green (Beyotime, China). The uptake of Exos was observed using a confocal laser scanning microscope (Zeiss LSM710, Germany).

2.6. Determination of cell viability

Cell viability was quantitatively evaluated by Cell Counting Kit-8 (Beyotime, China). In brief, chondrocytes (1×10^4) were planted in 96-well microculture plates incubated overnight. Then, the viability assay was conducted, and absorbance was assessed using a microplate reader at a wavelength of 450 nm according to the manufacturer's instructions with some modification. Three independent experiments were performed, and cell viability of different groups was evaluated as a percentage of the control.

2.7. Migration assay

Migration in conditioned chondrocytes was detected using a Transwell system. Briefly, 5×10^4 chondrocytes were placed in a 24-well transwell plate with 8 μm pore size inserts (Corning, NY, USA). Then, 500 μL of DMEM containing 0.5% FBS and 1% PBS with 5 μg Exos was added to the lower chamber before culturing for 16 h. The cells in the upper chamber (2×10^5 cells) were then placed in 4% paraformaldehyde for 20 min and mixed with 0.5% hematoxylin and eosin for 10 min. The percentage of cell migration in each well was determined in a blinded manner.

2.8. Cell apoptosis analysis

Chondrocytes were plated in 6-well plates at a concentration of 2×10^5/well and were treated with or without ADSC-Exo (5 μg). Cell apoptosis was analyzed by using an Annexin V assay kit (Keen, China) and then measured by a Beamcyte-1026® flow cytometer (BDA Inc., China).

2.9. Exosomal small RNA sequence assay

The small RNA sequence for $hADSCs^{ScAT}$ Exos and $hADSCs^{IPFP}$ Exos were performed by OE Biotech Company (Shanghai, China). Three samples were processed for each type of Exos. The fragmentation mixtures were hybridized to an Agilent-Human microRNA array 21.0 (8 × 60 K, Design ID:070,156). For microarray analysis, the Affymetrix (Santa Clara, CA, USA) miRNA 4.0 platform was employed. The sample labeling, microarray hybridization and washing were performed based on the manufacturer's instructions (Agilent Technologies Inc., Santa Clara, California, USA). Differentially expressed miRNAs were identified using a fold change cut off value of ≥1.5 set for both up- and down-regulated genes.

2.10. Luciferase reporter assay

Luciferase vectors including the 3′-UTR of ADAMTS4 containing the ADAMTS4-miR-99 b-3p response elements and the mutant were obtained from GenePharma. Either miR-99 b-3p mimic and negative control was then transfected into the human embryonic kidney (HEK) 293 cells in the presence of either the wild-type or the mutant reporter plasmid. Luciferase activity was determined with the Dual-Luciferase reporter system (Vazyme, China), and Renilla luciferase activity was set as internal control.

2.11. miRNA expression and transfection, miRNA abundant exos isolation

MiR-99 b-3p-mimic, miR-mimic-NC, were constructed by RiboBio (Guangzhou, China). The ADSCs and chondrocytes were transfected with mimics at a density of 4×10^5 each well in six-well plates using Lipofectamine 2000 reagent (Invitrogen, USA).

The Exos derived from miR-99 b-3p-mimic transfected ADSCs were isolated as previously described.

2.12. Plasmid transfection assay

The pcDNA3.1 vector and pcDNA3.1 vector for ADAMTS4 overexpression commercially were prepared by General Biosystems (GenePharma, China). These plasmids were transfected into chondrocytes with the Lipofectamine 2000 (Invitrogen, Carlsbad, CA, USA).

2.13. Hydrogel rheological characterization and in vitro degradation test

Rheological properties of the samples were assessed using a stress-controlled rheometer (HAAKE RheoStress 1, Thermo Scientific, USA) fitted with an 8 mm diameter flat plate (2 mm gap) at 25 °C. Prior to rheological testing, the granular hydrogel prepared by centrifuging HMP dispersion at 10^4 rpm for 15 min were carefully pipetted into the plate gap. Dynamic oscillatory strain amplitude sweep measurement was conducted by varying % strain from 0.1 to 1000% at a frequency of 1 Hz, and oscillatory frequency sweeps were conducted ranging from 0.1 to 100 rad/s at 1% strain amplitude.

For in vitro degradation analysis, each sample were put into PBS (pH = 7.4), PBS contained hyaluronidase (200U/ml) and PBS contained H_2O_2 (5 mM) respectively, at 37 °C and then placed in the shaker at 60 rpm. The supernatant was removed, and the solution was replenished at 2-day intervals. At predetermined time points, the residual weight of the sample was measured and compared with its initial weight. Each group was repeated for three parallel tests to ensure data validity. The degradation rate (%) of the HMPs was calculated based on the following equation.

2.14. Exos encapsulation efficiency and release test

The amount of remaining Exos in the solution was detected by BCA protein assay. The following formulas were used for calculating the Exos encapsulation efficacy (EE).

The release of Exos from HMP-exos was further carried out. Each sample was immersed in PBS (pH = 7.4), PBS contained hyaluronidase (200U/ml) (Aladdin, China) and PBS contained H_2O_2 (5 mM) (Aladdin, China) respectively, at 37 °C and then placed in the shaker at 60 rpm. At each determined time point (2-day intervals), supernatant was collected and fresh solution was added. Then, the released profile was calculated as released percentage across time. The Exos release percentage (%) was calculated by the following equation.

2.15. Cell cytotoxicity and compatibility

Chondrocytes were seeded in a 96-well plate at a density of 1×10^4 cells/well and cultured overnight, HMPs, HMPs@Exos^{ScAT}, HMPs@Exos$^{ScAT-99b-3p}$ were added to each well. After 24 h, cell viability was conducted using the Cell Counting Kit-8 (CCK-8, Beyotime, China) assay.

In addition, the cyto-compatibility was assessed by Calcein AM/PI staining assay. Chondrocytes at passage three were seeded in 24-well plates at a density of 5×10^4 cells/well and cultured overnight prior to the addition of 1–5 mg/mL. After 1, 2, and 3 days, the viability of the cells was analyzed using the Calcein/PI Cell Viability/Cytotoxicity Assay Kit (Beyotime, China).

2.16. Immunofluorescent staining

For cell immunofluorescence, chondrocytes were incubated in complete culture medium with various Exos for an additional 3 h. The cells were then washed in phosphate-buffered saline (PBS) and fixed with 4% paraformaldehyde for 15 min. The fixed cells were permeabilised with 0.1% Triton X-100 for 5 min and washed with PBS three times. Then, the cells were treated with primary ADAMTS4, ACAN, COMP antibodies (Abcam, Cambridge, UK) overnight at 4 °C in PBS supplemented with 1% bovine serum albumin.

2.17. Quantitative real-time polymerase chain reaction (RT-qPCR)

After harvesting the chondrocytes and separating the total RNA by TRIzol Reagent (Invitrogen, USA), and reverse transcribed into complementary DNA according to the manufacturer's protocol of the reverse transcription kit (R312, Vazyme, China). qPCR was carried out following the instructions provided by the Taq Pro Universal SYBR qPCR Master Mix (Q712, Vazyme, China) using a real-time fluorescence quantitative PCR appliance (QuantStudio®5, ThemoFisher Scientific, USA). Otherwise, the expression of miRNAs was quantified by miRNA Universal SYBR qPCR Master Mix (Vazyme, China) and miRNA 1st Strand cDNA Synthesis Kit (Vazyme, China) was applied for the single stranded cDNA synthesis. GAPDH and U6 were taken as internal reference genes. All the primers for RNAs are listed in Supplementary Table 1.

2.18. Western blot analysis

The proteins were harvested and lysed in RIPA buffer. Equal amounts of protein extracts (30 μg) were loaded per lane and resolved by SDS/PAGE. Subsequently, polypeptides were separated and transferred to PVDF membranes. The membranes were blocked and then treated overnight with rabbit anti-Col2a1 (1:1000, Abcam, UK), rabbit *anti*-MMP13 (1:1000, Cell Signaling Technology), rabbit *anti*-ACAN (1:1000, Abcam, UK), rabbit anti-COMP (1:1000, Abcam, UK), rabbit *anti*-ADAMTS4 (1:1000, Abcam, UK), and mouse *anti*-GAPDH (1:1000, Beyotime, China) antibodies, respectively. After being washed with TBST three times, the membranes were incubated using the corresponding HRP-conjugated secondary antibodies (1:1000, Beyotime, China) with blocking solution at room temperature for 2 h. Finally, the expression levels of protein were measured by enhanced chemiluminescence kit (Millipore, USA). The protein bands were normalized by GAPDH and quantified as the ratio of the optical density.

2.19. Induction of OA

All animal experiments were in accordance to the Animal Research Committee regulations of Nanjing first hospital, Nanjing medical university. OA was induced in 8-week-old male C57BL/6 mice by surgical destabilization of the medial meniscus (DMM) of the right knee. Specifically, the DMM surgery was performed by surgical sectioning of the medial meniscotibial ligament and the sham operation was performed by incision of the cutaneous and muscular planes at baseline.

2.20. Intra-articular injection

In the animal section 1 in Fig. 2, all mice underwent DMM surgery or sham surgery were randomly divided into three groups: (1) PBS group (control); (2) $Exos^{ScAT}$ group; (3) $Exos^{IPFP}$ group; (4) $Exos^{ScAT-NC}$ group; (5) $Exos^{ScAT-99b-3p}$ group. The mice were given intra-articular injections of 10 μl PBS or 10 μl Exos (5 μg) twice a week for 4 weeks with a 30-gauge needle and a micro syringe (Hamilton). Afterward the mice were sacrificed, and cartilage tissue was dissected for histological assessment (H&E, Safranin O/fast green and toluidine blue staining) and immunofluorescent staining (ADAMTS4, ACAN, COMP, Col2a1).

In the animal section 2 in Fig. 6, all mice underwent DMM surgery were randomly divided into five groups: (1) PBS group (Control); (2) $Exos^{ScAT-99b-3p}$ group; (3) HMPs group (4) $HMPs@Exos^{ScAT}$ group; (5) $HMPs@Exos^{ScAT-99b-3p}$ group. The mice were injected with 20 μl PBS, 20 μl $Exo@^{ScAT-99b-3p}$ (20μg), 30 μl HMPs, 30 μl HMPs@Exos (containing 20 μg Exos), 30 μl $HMPs@Exos^{ScAT-99b-3p}$ (containing 20 μg Exos) at the first day. After 4 and 8 weeks, the mice were sacrificed, and cartilage tissue was dissected for histological assessment (H&E, Safranin O/fast green and toluidine blue staining) and immunofluorescent staining (ADAMTS4, ACAN, COMP, Col2a1).

2.21. Statistical analysis

All data were expressed as mean ± standard deviation. One-way analysis of variance (ANOVA) followed by Tukey multiple-comparison

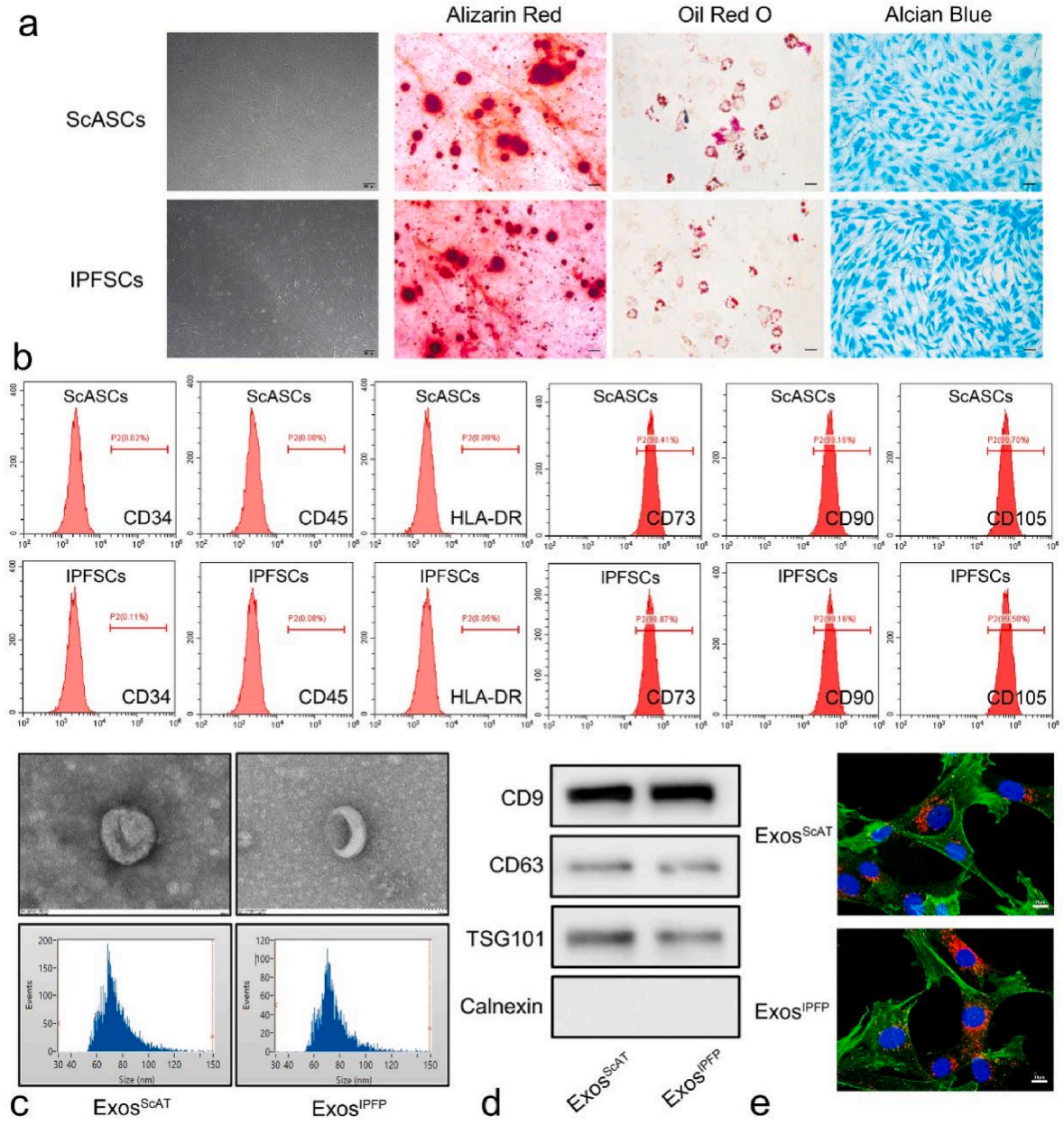

Fig. 1. Identification of ADSCs and ADSCs-derived Exos. (a) ADSCs displayed a representative spindle-like morphology. Identification of osteogenic, chondrogenic and adipogenic cells by Alizarin red staining, oil red staining and Alcian blue staining respectively. Scale bar: 200 μm. (b) Flow cytometry analysis of the cell surface markers on ADSCs, Results showed negativity for CD34, CD45, and HLA-DR and positivity for MSCs markers CD73, CD90, and CD105. (c) Morphology of ADSCs-derived Exos observed by transmission electron microscopy (TEM). Scale bar:100 nm. Particle size distribution and concentration of ADSCs-derived exosomes measured by NTA. (d) The surface markers of ADSCs-derived exosomes (CD9, CD63, TSG101 and Calnexin) were detected by western blot. (e) Uptake of the red fluorescence dye PKH26 labelled Exos into chondrocytes. Scale bar: 10 μm. (For interpretation of the references to color in this figure legend, the reader is referred to the Web version of this article.)

posthoc test was conducted to evaluate significant differences between groups. Statistical significance was considered at × $p < 0.05$.

3. Results

3.1. Isolation and identification of hADSCs^{ScAT} and hADSCs^{IPFP}

We obtained human IPFP tissues and ScAT tissues from OA donors with total knee arthroplasty and isolated MSCs according to the methods described in previous study. Then, the isolated ADSCs were observed under an optical microscope, and the image in Fig. 1a shows that the two kinds of ADSCs displayed typical MSC morphology with a spindle-like shape. Moreover, flow cytometry analysis showed that more than 95% of these cells expressed classical MSC markers, including CD73, CD90, and CD105, while no cells expressed haematopoietic markers, such as CD34, CD45, and HLA-DR (Fig. 1b), indicating a high enrichment of ADSCs. Next, we used an in vitro differentiation assay to further investigate whether these cells have the potential to differentiate into adipocytes, osteocytes, and chondrocytes. Osteogenic potential was confirmed by the staining of calcium mineral deposits with Alizarin Red

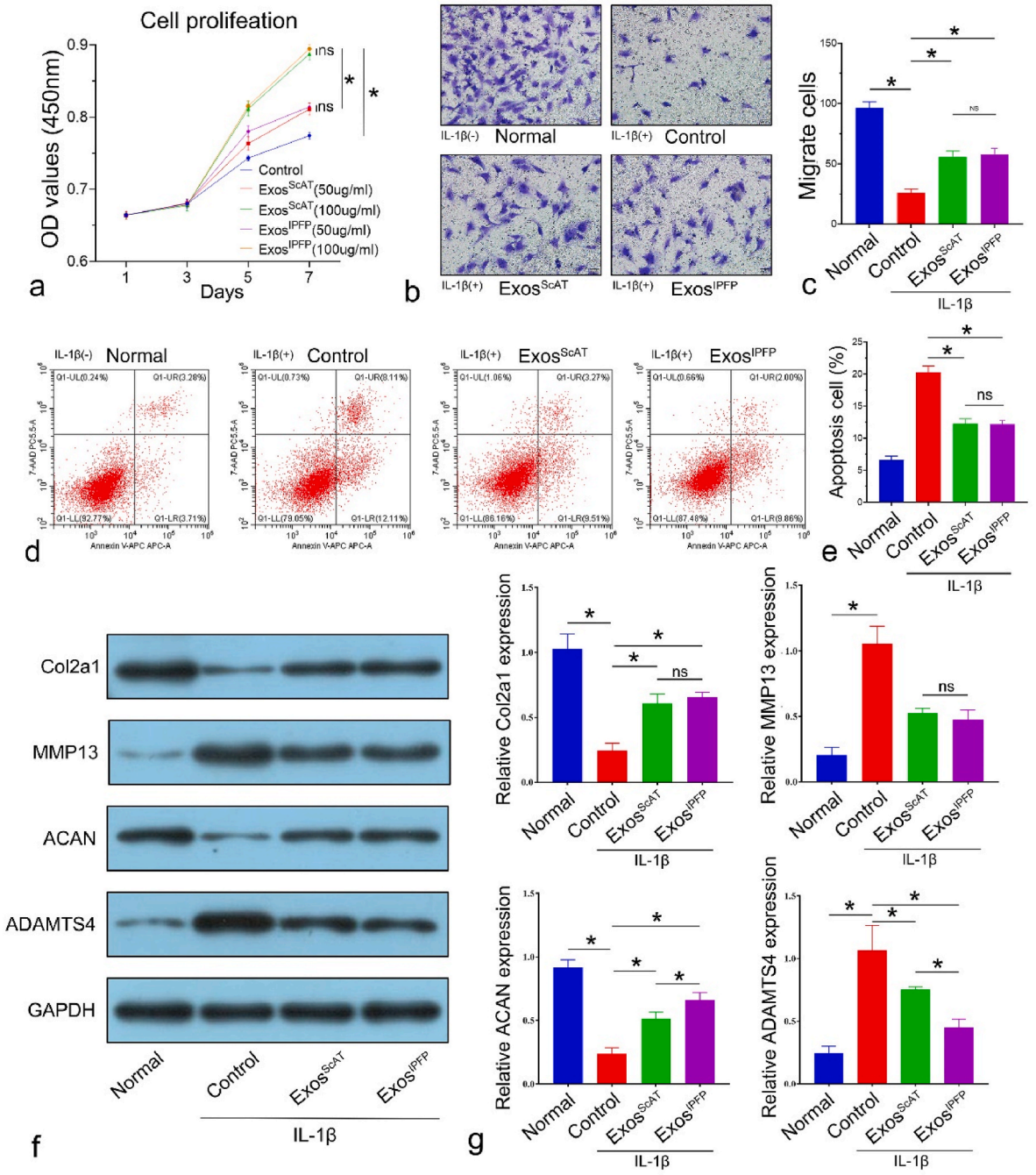

Fig. 2. ADSCs-Exos promote proliferation, migration, anabolism, inhibit apoptosis and catabolism in osteoarthritic chondrocytes. (a) CCK-8 assays were used to detect proliferation with Exo^{ScAT} or Exos^{IPFP} treatment in osteoarthritic chondrocytes. (b ~ c) Transwell assays were performed to examine the migration with Exo^{ScAT} or Exos^{IPFP} treatment in osteoarthritic chondrocytes (scale bar: 20 μm). (d ~ e) Flow cytometry was used to analyze apoptosis in osteoarthritic chondrocytes with Exo^{ScAT} or Exos^{IPFP} treatment. (f ~ g) Protein expression levels of Col2a1, MMP13, ACAN and ADAMTS4 of osteoarthritic chondrocytes with Exo^{ScAT} or Exos^{IPFP} treatment was examined using Western blot analysis. *$p < 0.05$, ns: no significance.

(Fig. 1a), while adipogenic potential was evaluated by the observation of small cytoplasmic lipid droplets stained with Oil Red O (Fig. 1a). Chondrogenic potential was confirmed by staining with sulfated glycosaminoglycans using Alcian Blue (Fig. 1a).

3.2. Isolation and identification of exos derived from $hADSCs^{ScAT}$ and $hADSCs^{IPFP}$

Transmission electron microscopy (TEM), nanoparticle tracking analysis (NTA) and western blotting were used to characterize the Exos secreted from ADSCs. TEM clearly revealed that Exos exhibited a cup-shaped or round morphology with a diameter of 50–150 nm (Fig. 1c). NTA showed that most of these vesicles ranged from 30 to 150 nm in size (Fig. 1c). Western blotting analyses indicated that Exo^{ScAT} and Exo^{IPFP} expressed exosomal markers such as CD9, CD63, and TSG101 (Fig. 1d).

3.3. Uptake of ADSC-exos by chondrocytes

The laser confocal microscopy image showed the accumulation of Exos in chondrocytes. The nuclei of chondrocytes were stained with DAPI (blue), actin of chondrocytes was stained with phalloidin-FITC (green), and the Exos were labelled with PKH26 (red). The Exos were observed in the perinuclear region of the chondrocytes (Fig. 1e), confirming the successful internalization of ADSC-Exos by chondrocytes. Moreover, there was no difference between $Exos^{ScAT}$ and $Exos^{IPFP}$ internalized by chondrocytes according to the fluorescence intensity.

3.4. ADSC-exos promote proliferation, migration, and anabolism and inhibit apoptosis and catabolism in osteoarthritic chondrocytes

To investigate whether ADSC-exos alleviate OA by targeting chondrocytes, we harvested $Exos^{ScAT}$ and $Exos^{IPFP}$; we added different Exos at concentrations of 50 μg/mL and 100 μg/mL to IL-1β (10 ng/mL)-treated chondrocytes cultures for 7 days. The results from CCK-8 assays showed that the proliferation of chondrocytes was stimulated by Exos in a dose-dependent manner (Fig. 2a); however, there was no significant difference between $Exos^{ScAT}$ and $Exos^{IPFP}$ at the same concentration (Fig. 2a). Transwell assays and Annexin V-FITC/PI staining were performed to evaluate migration capacity and apoptosis in IL-1β (10 ng/mL)-treated chondrocytes. The results showed that Exos promoted chondrocyte migration and inhibited chondrocyte apoptosis; however, no significant difference between $Exos^{ScAT}$ and $Exos^{IPFP}$ was observed (Fig. 2b ~ e). Furthermore, we measured the protein levels of anabolism-related genes (collagen II and aggrecan) and catabolism-related genes (MMP13 and ADAMTS4), which are highly related to OA pathological processes. IL-1β treatment significantly decreased collagen II and aggrecan expression, while it increased the protein levels of MMP13 and ADAMTS4. The coculture of Exos with chondrocytes reversed the effect of IL-1β on aggrecan and ADAMTS4. Interestingly, the expression of aggrecan in the Exo^{IPFP} group was higher than that in the Exo^{ScAT} group, while Col2a1 and MMP13 levels were similar in the two groups (Fig. 2f and g).

3.5. MiR-99 b-3p is upregulated in Exo^{IPFP} and plays a critical role in maintaining anabolism in articular chondrocytes

To further investigate the mechanism by which Exos affect chondrocytes, we isolated RNA from $Exos^{IPFP}$ and $Exos^{ScAT,}$ performed small RNA sequencing of the miRNAs derived from the Exos and compared them between the two groups (Fig. S1a). According to the sequencing results, we identified the 10 miRNAs that had the most obvious upregulation and further verified them in the Exo fractions by RT−qPCR. These results showed that miR-99 b-3p was the most upregulated miRNA in $Exos^{IPFP}$ (Fig. S1b).

3.6. MiR-99 b-3p regulates ADAMTS4 by directly targeting the 3′-UTR

To identify the target gene for miR-99 b-3p, the potential regulatory relationship between mRNA and miRNAs was predicted using the TargetScan, miRWalk, miRTarBase, and miRPathDB databases. Because the changes in chondrocytes mainly occur in aggrecan, one of the components of the ECM, we searched the gene set related to ECM expression in the GO database (GO:0031,012). Then, we calculated Venn diagrams (Fig. S1c) to identify the overlap between different genes and miRNA data in the database, and we predicted that ADAMTS4 was a potential target of miR-99 b-3p. As shown in Fig. S1d, miR-99 b-3p has one potential complementary sequence with ADAMTS4. A luciferase reporter assay was used to confirm the direct target of miR-99 b-3p, as shown in Fig. S1e. The luciferase activity of ADAMTS4-WT was suppressed when the cells were cotransfected with the miR-99 b-3p mimic, while this effect was not observed for ADAMTS4-MUT, suggesting that ADAMTS4 is a direct target of miR-99 b-3p.

The expression of miR-99 b-3p was markedly reduced in OA cartilage compared to normal cartilage (Fig. 3a). However, higher protein levels of ADAMTS4 were observed in OA cartilage than in normal cartilage (Fig. 3b and c) Moreover, in IL-1β induced chondrocytes, miR-99 b-3p expression was decreased (Fig. 3d), and ADAMTS4 protein levels were increased (Fig. 3e ~ f).

Histological staining of cartilage in OA patients and normal patients showed that the cartilage surface of OA patients was severely worn, and safranin O/fast green staining indicated a great loss of glycosaminoglycan in OA cartilage (Fig. 3h). Through immunohistochemical staining, we found that the expression of ADAMTS4 in OA cartilage was significantly higher than that in normal cartilage, while the expression of ACAN and COMP was significantly lower in OA samples (Fig. 3i).

3.7. MiR-99 b-3p promotes cartilage-related protein expression by targeting ADAMTS4 in vitro

Chondrocytes were transfected with miR-99 b-3p mimic and miR-NC, miR-99 b-3p expression was assessed by RT−qPCR, and we discovered that the miR-99 b-3p mimic elevated miR-99 b-3p expression nearly 8 times compared with the NC group (Fig. S2a). ADAMTS4 expression was quantified using western blot analysis (Figs. S2b and c). The results showed that ADAMTS4 expression was reduced by the miR-99 b-3p mimic. To further explore the relationship between miR-99 b-3p and ADAMTS4, in vitro rescue experiments were performed. We transfected the miR-99 b-3p mimic or miR-NC into chondrocytes and then cotransfected the chondrocytes with a plasmid that overexpresses ADAMTS4 (pcDNA-ADAMTS4) or with pcDNA-NC. The results showed that upregulating miR-99 b-3p restored the protein levels of ACAN and COMP inhibited by pcDNA-ADAMTS4. Together, these results demonstrated that miR-99 b-3p targets and negatively regulates ADAMTS4 (Fig. S2d-g), while miR-99 b-3p overexpression exhibited a positive effect on the expression of cartilage-related proteins that were inhibited by ADAMTS4 (Fig. S2d-g).

3.8. Overexpression of mir-99 b-3p increases anabolism-related protein expression more potently in $Exos^{ScAT}$ than in $Exos^{IPFP}$ in vitro

Next, the effect of ADSC-derived Exos on chondrocytes was investigated. ScASCs were transfected with miR-99 b-3p mimic and miR-NC, and miR-99 b-3p expression was assessed by RT−qPCR. The results showed that miR-99 b-3p expression in the IPFSCs group was approximately 3 times higher than that in the ScASCs group, while the $ScASCs^{miR-99b-3p}$ group was approximately 12 times higher than that in the ScASCs group (Fig. S3a). Then, we isolated Exos from the corresponding ADSCs and assessed miR-99 b-3p in all groups. Compared with the $Exos^{ScAT}$ and $Exos^{IPFP}$ groups, miR-99 b-3p expression increased more than 11-fold and 4-fold in the $Exos^{ScAT-99b-3p}$ group, respectively (Fig. S3b). Chondrocytes were stimulated with IL-1β for 24 h, followed

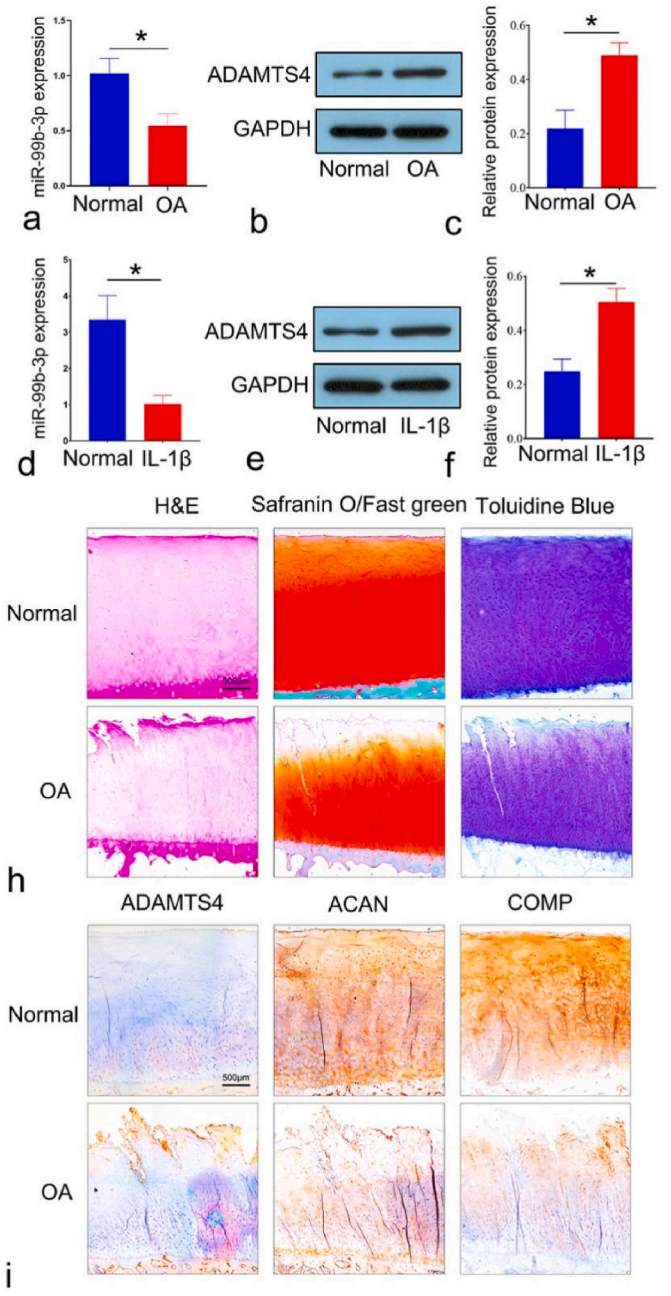

Fig. 3. The expression of ADAMTS4 is increased in osteoarthritic cartilage. (a) Expression of miR-99 b-3p in normal and OA cartilage tissues was determined by RT-qPCR. (b, c) Expression of ADAMTS4 in normal and OA cartilage tissues was determined by western blot. (d) Expression of miR-99 b-3p in normal and IL-1β induced chondrocytes was determined by RT-qPCR. (e, f) Expression of ADAMTS4 in normal and IL-1β induced chondrocytes was determined by western blot. (h) H&E, Safranin O/fast green, Toluidine Blue staining in normal and OA cartilage tissue. Scale bar: 250 μm. (i) Immunohistochemical staining (ADAMTS4, ACAC, COMP) in normal and OA cartilage tissue. Scale bar: 500 μm *p < 0.05. (For interpretation of the references to color in this figure legend, the reader is referred to the Web version of this article.)

by treatment with different kinds of Exos ($Exos^{ScAT}$, $Exos^{IPFP}$, $Exos^{ScAT-NC}$, $Exos^{ScAT-99b-3p}$) (Fig. S3c). The results showed that the expression of ADAMTS4 was lower in all Exos treatment groups than in the control group. The $Exos^{IPFP}$ group was lower than the $Exos^{ScAT}$ group, while the $Exos^{ScAT-99b-3p}$ group had the lowest expression. Additionally, the expression of ACAN and COMP was higher in all treatment groups than in the control group, and the expression in the $Exos^{ScAT-99b-3p}$ group was significantly higher than that in the $Exos^{ScAT}$ and $Exos^{IPFP}$ groups (Fig. 4ã d).

3.9. Overexpression of mir-99 b-3p in $Exos^{ScAT}$ promoted cartilage regeneration in murine DMM models

We evaluated the effects of intra-articular injected Exos treatments in mice with OA by histological assessment (Fig. 5a). Four weeks after the DMM operation, the knee joint specimens of animals were collected for H&E, Safranin O/Fast Green staining and Toluidine blue staining (Fig. 5b). In the control group, the cartilage surface was rough and badly worn, the articular cartilage was thin or even missing, and the subchondral bone was exposed and destroyed. Moreover, significant loss or thinning of the proteoglycans was observed in the control group. The cartilage surface in the $Exos^{ScAT}$ and $Exos^{IPFP}$ groups was relatively smooth compared to that in the control group, which had no exposed subchondral bone and increased proteoglycan content; the proteoglycan distribution of the $Exos^{IPFP}$ group was more uniform and denser. However, the $Exos^{ScAT-99b-3p}$ group showed the best repair effect, the cartilage surface was smooth, the cartilage thickness was uniform, there were no cracks on the surface; the subchondral bone was well reconstructed, the cells in the repaired tissue were clearly arranged in a vertical column, and the proteoglycan content was significantly higher than that in the other groups, with a uniform distribution. Histological scores, OARSI grade, and Mankin's scores (Fig. 5c–e) in DMM knees were assessed to quantify the extent of cartilage injury, and the data showed that $Exos^{ScAT-99b-3p}$ exhibited a more evident protective influence on cartilage repair after DMM surgery (Fig. 5c ~ e).

The levels of ADAMTS4, ACAN, COMP, and Col2a1 in the repaired tissue were verified by immunofluorescence staining. With the increased expression of miR-99 b-3p in chondrocytes, the expression of ADAMTS4 was decreased, while the expression of ACAN and COMP was increased (Fig. 5f) In other words, the expression of ADAMTS4 was lowest; moreover, ACAN and COMP levels were significantly higher in the $Exos^{ScAT-99b-3p}$ group than in the other groups (Fig. 5f). The results showed that overexpression of miR-99 b-3p in Exos can attenuate OA by downregulating ADAMTS4 protein in vivo.

3.10. Characterization of HMPs

The synthesis methodology of HB-PEGDA and SH-HA is depicted in Fig. 6a and b. As shown in Fig. 6d, HMPs and HMPs@Exos were prepared by microfluidic technology, and gelation formed spontaneously through the thiol-ene Michael addition reaction (Fig. 6c). The characteristics of the as-obtained products collected at different time points are shown in Fig. 6e and f. A unimodal weak peak with Đ (Mw/Mn) < 1.5 was detected after 1 h of reaction, and then the molecular weight of the polymer steadily increased with time. As the reaction proceeded at 70 °C over 5 h, the molecular weight of the HB-PEGDA polymer increased dramatically with time, and a broad Đ was observed, indicating the formation of HB-PEGDA polymers with hyperbranched structures (Fig. 6g). The PBA-HB-PEGDA polymer with a molecular weight of 15 kDa was used for the following HMP synthesis.

Rheological studies revealed that the storage modulus values (G′) for all three formulations were higher than the loss modulus values (G″). Moreover, all the samples showed a linear viscoelastic region at low strain percentages with G′ independent of the applied deformation (Fig. 6h). These characteristics indicate that the as-obtained granular hydrogels behaved like viscoelastic gels. Additionally, by controlling the HB-PEGDA:SH-HA ratio, the mechanical properties of the granular hydrogels composed of HMPs can be readily tuned with G' values varying from 60 to 400 Pa, facilitating the mimicking of mechanical variability in a range of soft tissues (Fig. 6i).

The obtained HMPs and HMPs@Exos were observed under a bright-field microscope (Fig. 7a), with the majority of particles being approximately 120 μm in diameter (Fig. 7b) (see Fig. 8).

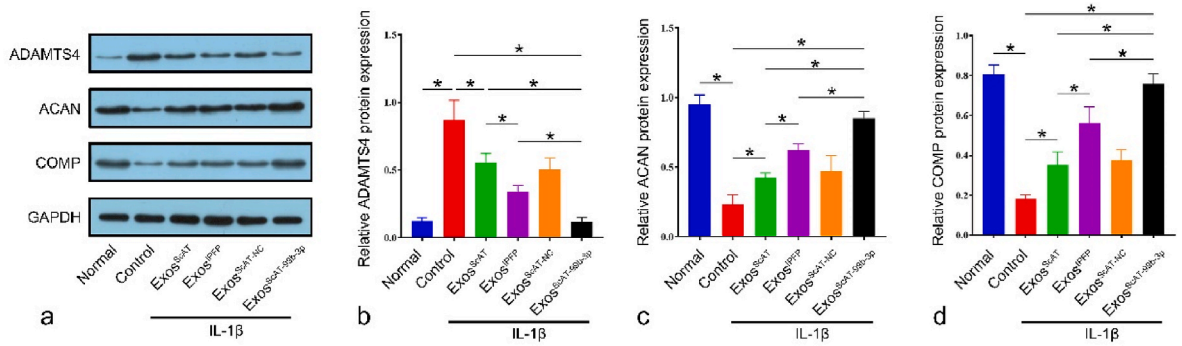

Fig. 4. Normal and IL-1β induced chondrocytes were co-cultured with Exos, (ād) ADAMTS4, ACAN, COMP expression levels were measured by western blotting. *p < 0.05.

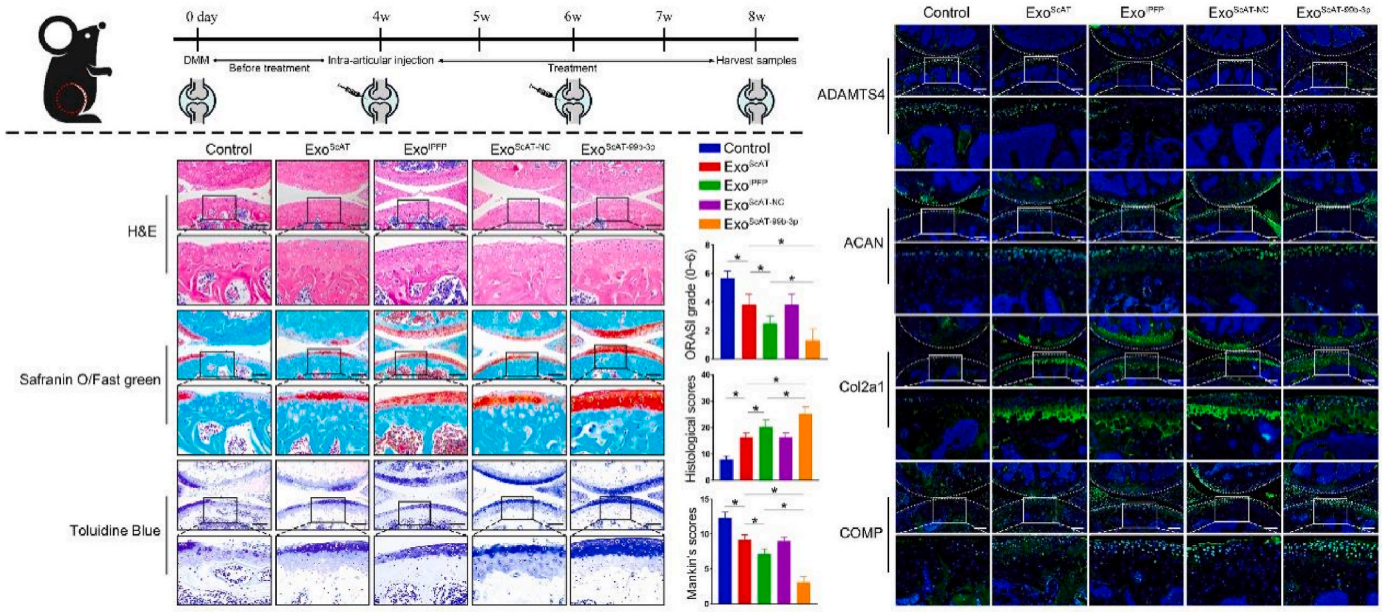

Fig. 5. Overexpression miR-99 b-3p in Exos^{ScAT} promote cartilage regeneration in Mice DMM Model. (A) A flow diagram showing the time of intra-articular injection. (B) H&E, Safranin O/fast green, Toluidine Blue staining of mice knee joints. Scale bar = 200 μm. (C) OARSI grade of the knee joints of DMM mice. (D) Histological scores of the knee joints of DMM mice. (E) Mankin's scores of the knee joints of DMM mice. (F) Immunofluorescence analysis of ADAMTS4, ACAN, COMP and Col2a1 in knee joints of DMM mice. Scale bar = 200 μm *p < 0.05. (For interpretation of the references to color in this figure legend, the reader is referred to the Web version of this article.)

As illustrated in Fig. 7c, the HMPs possess excellent injectability and can fabricate arbitrary 2D patterns with an extrusion-based 3D printer with a 26-gauge needle.

3.11. Exos loading, distribution, release, and HMPs degradation

After labelling PEGDA with fluorescein O-methacrylate and labelling Exos with PKH26, HMPs were prepared. Confocal microscopy showed that the microspheres were uniformly distributed green, and the Exos were uniformly distributed in red dots (Fig. 7f). The results showed that PEGDA and Exos were intact and uniformly distributed in the microparticles. Hyaluronidase can act on β-*N*-acetylhexosamine-1,4 glycosidic bonds, leading to the degradation of microparticles [54–56]. The encapsulation efficiency of Exos in HMPs was 78.5 ± 2.4%.

To investigate the degradation of HMPs in vitro, a degradation assay was carried out. During long incubation times, HMPs in hyaluronidase and H_2O_2 showed continuous and slow biodegradation within 26 days and 18 days, respectively. However, the HMPs exhibit long-term stability in PBS buffer until 30 days (Fig. 7d).

Consistent with degradation experiment, sustained release of exos was observed in solutions containing hyaluronidase (24 days) or H_2O_2 (16 days) (Fig. 7e). However, little release was measured in the PBS solution, indicating that the HMPs can serve as an effective drug delivery system for controlled drug release in the microenvironment of osteoarthritis.

3.12. Biocompatibility of HMPs in chondrocytes, release of exos from HMPs and exos uptake by chondrocytes

In the no contact coculture system (Fig. S4a), Exos, HMPs, and HMPs@Exos were added to the upper transwell chambers. The laser confocal microscope image (Fig. S4b) showed Exos uptake by chondrocytes. The amount of Exos taken up by chondrocytes in the Exo group was higher on day 1, and then the Exos uptake gradually decreased. At day 7, it was already difficult to detect Exos fluorescence in chondrocytes, whereas in the HMPs@Exos group, although the amount of Exos uptake by chondrocytes was relatively low on day 1, the fluorescence gradually increased in the following days, which was related to the gradual degradation of the hydrogel and the controlled release of Exos. Calcein AM/PI staining of chondrocytes was visualized under a

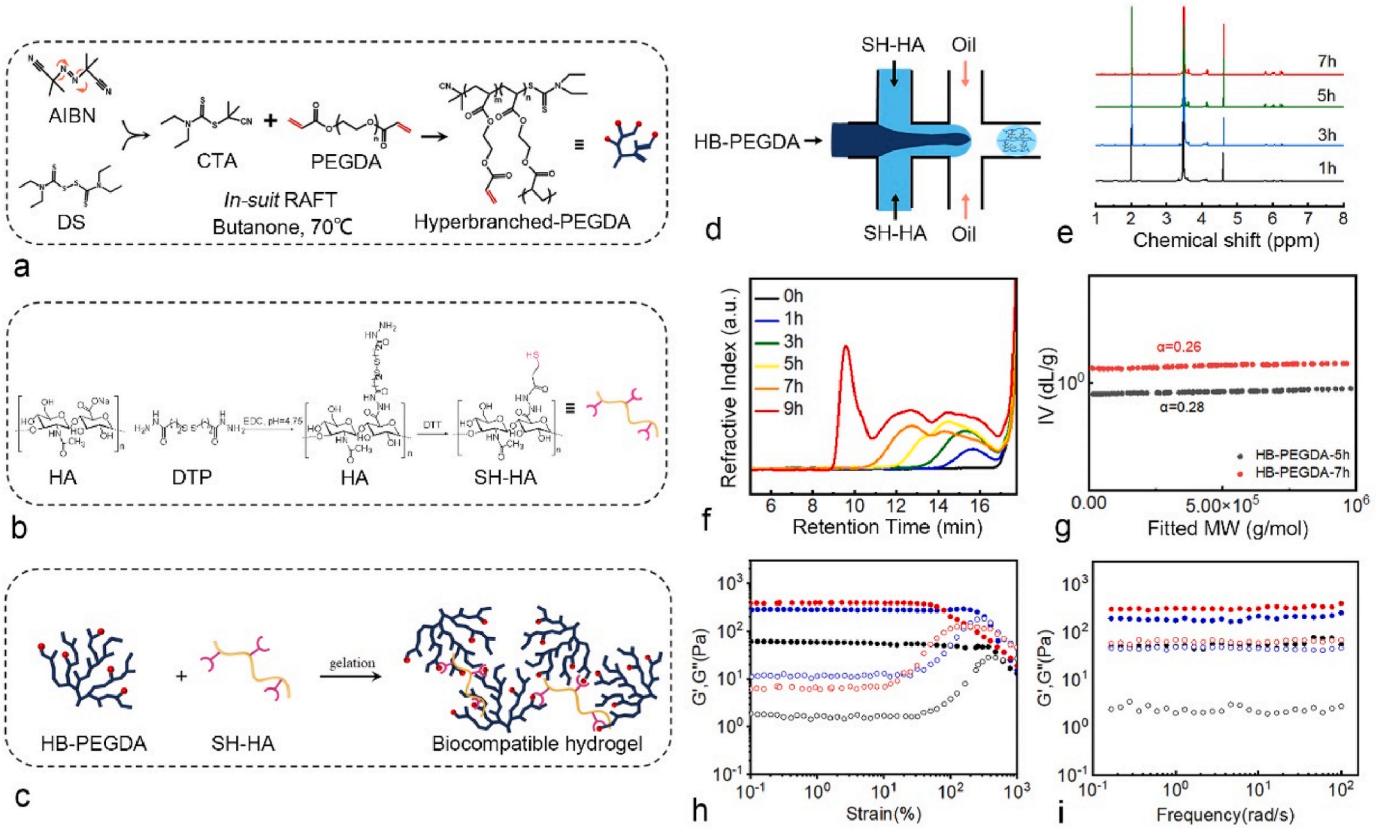

Fig. 6. (a) Schematic for the synthesis of HB-PEGDA. (b) Schematic for the synthesis of SH-HA. (c) The formation of the hydrogel via the thiol-ene Michael addition chemistry. (d) The fabrication of HMPs and HMP@Exos by microfluidic technology. (e) 1H NMR confirmed the formation of HB-PEGDA products. (f) GPC traces of HB-PEGDA polymers at different time points. (g) Mark-Houwink plots of the HB-PEGDA polymers isolated at the polymerization time of 5 and 7 h, respectively. (g ~ i) Oscillatory amplitude and frequency sweep test results of the granular hydrogels made of 3.33% (w/v) HB-PEGDA and 1%, 1.33%, or 1.66% (w/v) SH-HA, respectively.

fluorescence microscope; living cells showed green fluorescence, while dead cells showed red fluorescence. The results showed that chondrocytes exhibited good cell viability during 7 days of culture with a negligible number of dead cells (Fig. S4c). CCK-8 assay was used to assess the cytotoxicity of the HMPs in chondrocytes, revealing that the HMPs did not exhibit any significant cytotoxicity when used to treat chondrocytes, with survival rates remaining >90% (Fig. S5).

Additionally, in the contact coculture system (Fig. 8a), HMPs were cocultured directly with chondrocytes in petri dishes. The LSM images (Fig. 8b) showed that chondrocytes grew on the surface of the HMPs, and the cells of all groups gradually increased over time, while the number of cells in the groups with HMPs encapsulated with Exos was obviously higher than that in the HMPs group. All groups showed a green live cell fluorescence signal with few dead cells. After incubation for 7 days, DAPI/FITC-phalloidin fluorescence staining indicated that chondrocytes covered the HMPs surfaces with Exos uptake into cells (Fig. 8c).

3.13. Intraarticular retention and in vivo biological safety of HMP treatment

To determine the intraarticular retention of Exos with or without encapsulation in HMPs, the fluorescent signals were monitored using the IVIS system at 1, 3, 7, 14, and 28 days after intraarticular injection. The signals in both groups decreased over time; however, fluorescence was found in the HMPs@Exos and HMPs@Exos$^{ScAT-99b-3p}$ groups on the 28th day, while the signal in the Exos group was undetectable after the 7th day of injection (Fig. S6). These results demonstrated the instability and poor local retention ability of the Exos, but encapsulation in HMPs might improve these shortcomings.

To evaluate the biological safety of the HMPs in vivo, the main organs (heart, liver, spleen, lung, and kidney) were obtained from mice on day 28 after treatment and stained with hematoxylin and eosin (H&E). Comparisons with the control group showed no significant tissue damage or any inflammatory lesions in H&E staining of major organs from the groups (Fig. S7), suggesting that HMPs show good biocompatibility in vivo.

3.14. Expression of ADAMTS4 and its substrates (ACAN and COMP) in vitro

Next, the coculture of HMPs and chondrocytes was performed using Transwell plates to examine the effects of different HMPs groups. IL-1β-induced chondrocytes were treated with PBS, Exos$^{ScAT-99b-3p}$, HMPs, HMPs@Exos^{ScAT} and HMPs@Exos$^{ScAT-99b-3p}$. On the 14th day, the protein expression of ADAMTS4, ACAN, and COMP was determined by immunofluorescence staining and western blotting. The expression of ADAMTS4, ACAN, and COMP in chondrocytes was detected by immunofluorescence (Fig. S9a). The results showed that the HMPs@Exos$^{ScAT-99b-3p}$ group expressed less ADAMTS4, while ADAMTS4 was significantly increased in the control and HMPs groups. However, the expression of ACAN and COMP was significantly enhanced in the HMPs@Exos$^{ScAT-99b-3p}$ group compared to that in the remaining groups, indicating that HMPs@Exos$^{ScAT-99b-3p}$ could effectively inhibit ADAMTS4 expression and promote ECM synthesis in chondrocytes by releasing miR-99 b-3p. Consistent with the IF results, the WB results showed that HMPs@Exos$^{ScAT-99b-3p}$ significantly inhibited ADAMTS4 protein expression and increased ACAN, COMP and collagen II protein

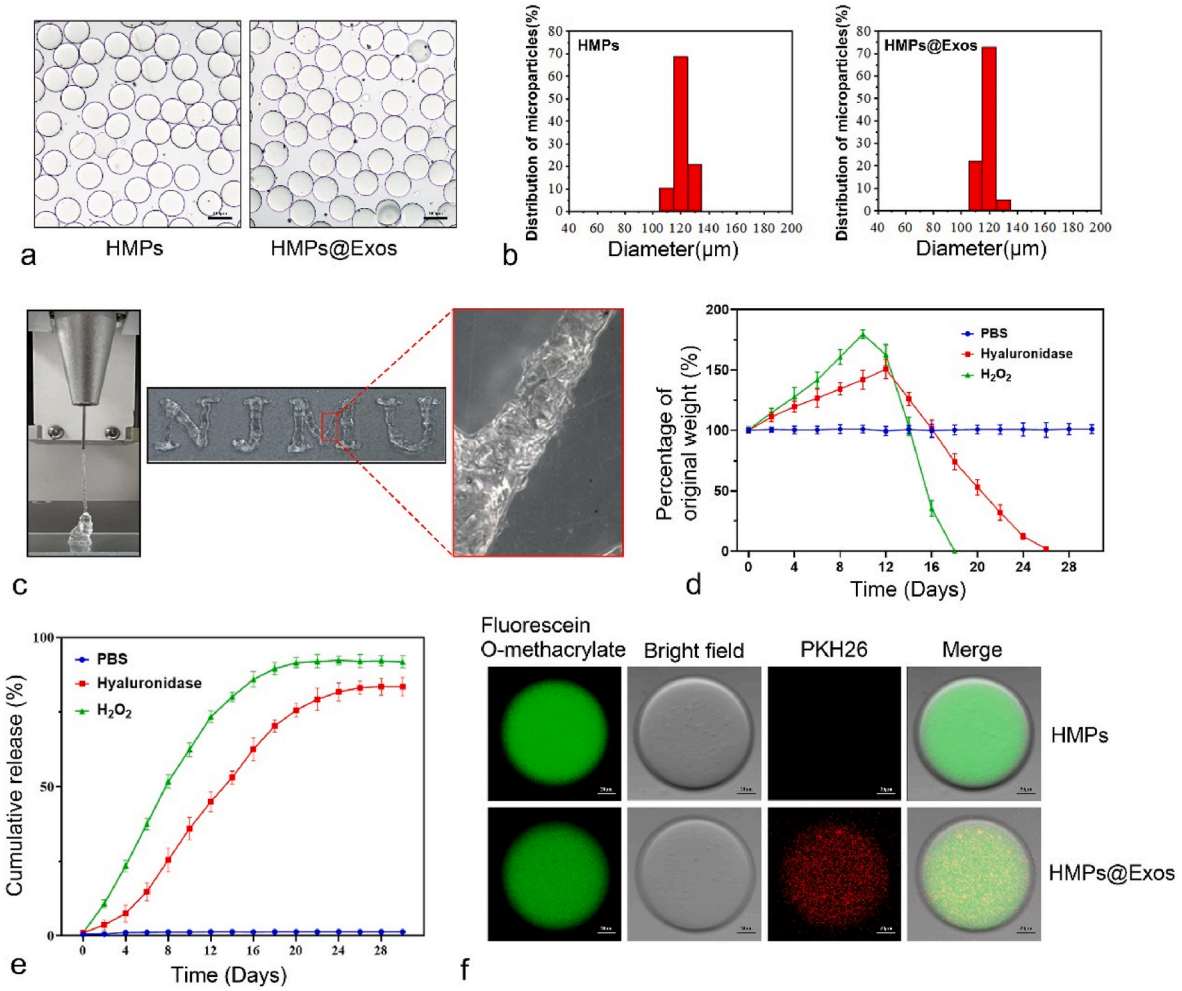

Fig. 7. Exos loading, distribution and HMPs Degradation. (a, b) Microscopic image and Diameter distribution of HMPs and HMPs@Exos. Scale bar = 100 μm (c) Photograph of the granular hydrogel filament while it is extruded from a 26 G conical nozzle, The injected patterns of "NJMU". (d) The degradability of HMPs in different conditions. (e) Exos release profiles of the HMPs@Exos in different conditions. (f) Fluorescence images of HMPs and HMPs@Exos, green fluorescence indicates HB-PEGDA, red fluorescence indicates Exos. Scale bar = 20 μm. (For interpretation of the references to color in this figure legend, the reader is referred to the Web version of this article.)

levels compared with those in the other groups on the 14th day of coculture (Fig. 9b ~ e).

3.15. In Vivo Therapeutic Effect of OA

To further investigate the protective effect of HMP-encapsulated Exos on cartilage degeneration, histological and immunofluorescence evaluations were performed at 4th-week and 8th-week after surgery (Fig. 10a). The articular cartilage in the control group (PBS) showed severe surface abrasion, disorganized chondrocytes, and weak toluidine blue and Safranin O/fast green staining. In comparison, the $Exos^{ScAT-99b-3p}$ group and $HMPs@Exos^{ScAT}$ group had relative integrity and regular cartilage structure compared with the PBS group, while the $HMPs@Exos^{ScAT-99b-3p}$ group showed the best morphological integrity and reduced erosion of cartilage surface destruction. According to the results of Safranin O/Fast Green and toluidine blue staining in the treatment groups, the amount of glycosaminoglycan was highest in the $HMPs@Exos^{ScAT-99b-3p}$ group, followed by the $HMPs@Exos^{ScAT}$ and $Exos^{ScAT-99b-3p}$ groups (Fig. 10b and c). The evaluation of histological scores, OARSI grade, and Mankin's scores at 8th week showed that the $HMPs@Exos^{ScAT-99b-3p}$ group had the best outcome for maintaining the cartilage ECM (Fig. 10c ~ e).

Finally, the protein expression levels of ADAMTS4, ACAN, COMP, and Col2a1 were measured (Fig. 10f). The results showed that ACAN, COMP, and Col2a1 protein expression was significantly decreased in the control group compared to the $Exos^{ScAT-99b-3p}$, $HMPs@Exos^{ScAT}$, and $HMPs@Exos^{ScAT-99b-3p}$ groups. Compared to that in the control group, the expression of ADAMTS4 in all the groups was decreased. However, the expression of ADAMTS4 treated with $HMPs@Exos^{ScAT-99b-3p}$ was the lowest, and the levels of ACAN, COMP, and Col2a1 were highest among all the OA models.

4. Discussion

Homeostasis of the articular cartilage is maintained via a delicate balance among a series of processes [38]. An increasing number of studies have shown that proteinases play an important role in the development of OA [38,39]. ADAMTS4, termed aggrecanase-1, is an important cartilage matrix–degrading enzyme that can degrade ECM components [40,41], which is also considered a marker of cartilage degeneration in inflammatory joint diseases such as OA [39]. ACAN and COMP are the main components of cartilage ECM, which provide cartilage with resistance to compressive stress [40]. Preventing ACAN loss by inhibiting aggrecanase activity can slow progressive cartilage erosion, which may delay or even prevent the development of end-stage OA [40]. Aggrecanase inhibitors have been identified as candidates for

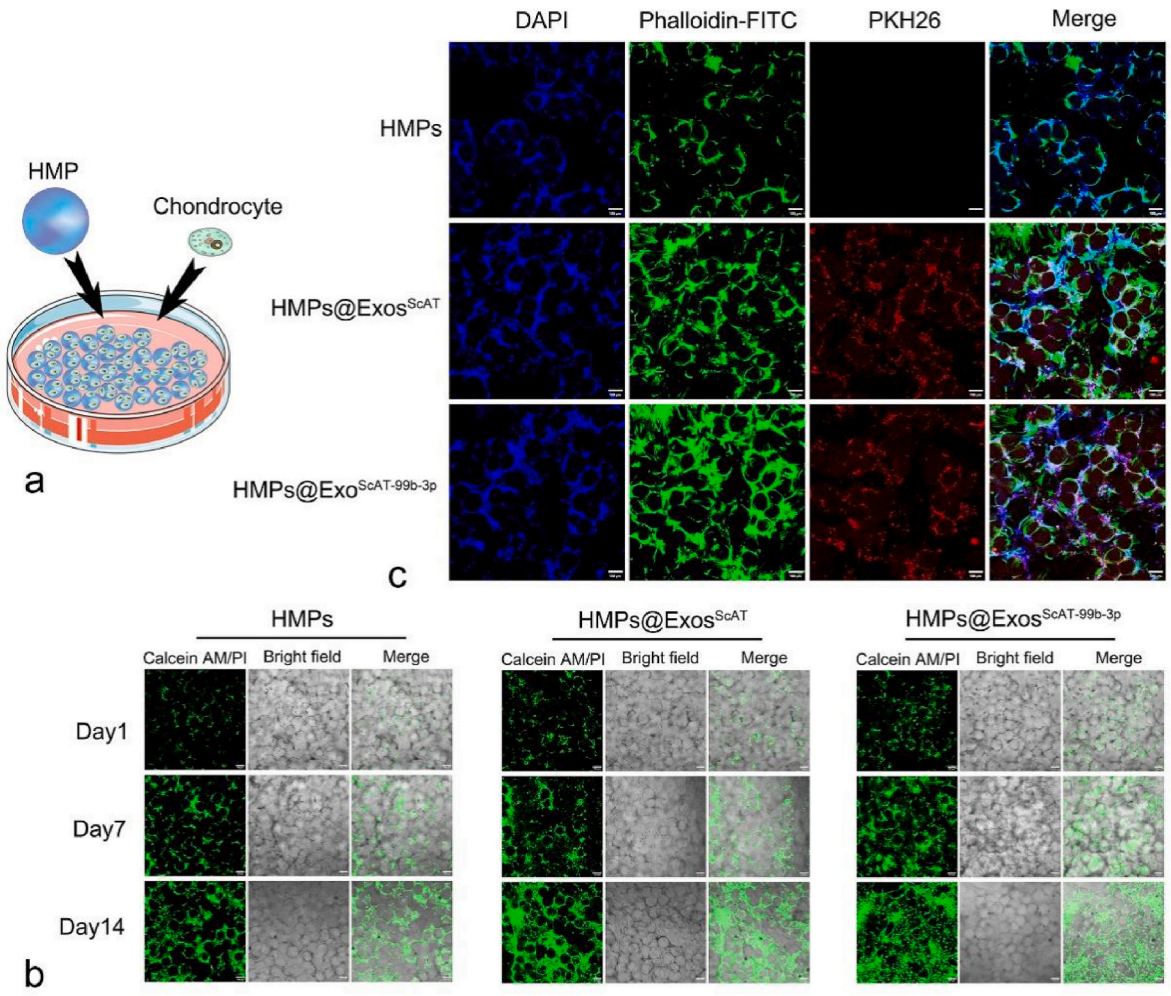

Fig. 8. Biocompatibility of HMPs in chondrocytes, release of exosomes from HMPs and exosomes uptake by chondrocytes. (a) The graphical illustration of contact co-culture system. (b) Images of Calcein AM/PI staining in normal, $Exos^{ScAT}$, HMPs, HMPs@Exos and $HMPs@Exos^{ScAT-99b-3p}$ groups on day 1,7,14. Scale bar = 100 μm (c) Images of phalloidin/DAPI/PKH26 staining in HMPs, HMPs@Exos and $HMPs@Exos^{ScAT-99b-3p}$ groups on day 7. Scale bar = 100 μm.

arthritis therapy in vivo [39,40]. Therefore, miR-99 b-3p may be a tool that can be used to maintain ECM stability by inhibiting ADAMTS4 expression. However, naked miRNA is susceptible to degradation by RNase in the extracellular environment [42], Exos was used to deliver miR-99 b-3p which can be phagocytosed by chondrocytes to regulate cell function [24,27].

In clinical therapy, ADSCs are superior to other cells because of their lower immune rejection potential, abundant sources, safety and low cost [9,10]. Although both IPFP and ScAT belong to adipose tissue, their corresponding stem cells have been reported to exhibit differences in the treatment of OA, reasearchers pay more attention to the Exos secreted by IPFSCs, but the source of IPFP is limited and inflammatory phenotype may severe, however, the content of ScAT is rich, which is an ideal source for extracting stem cells and Exos. By using an IL-1β induced in vitro OA model, we demonstrated that $Exos^{ScAT-99b-3p}$ have significantly greater efficacy in alleviating chondrocyte degradation than $Exos^{IPFP}$ and $Exos^{ScAT}$. The chondroprotective effect of $Exos^{ScAT-99b-3p}$ may in part be attributed to the downregulation of ADAMTS4. An in vivo experiment using a DMM OA model confirmed that IA injection of $Exos^{ScAT-99b-3p}$ resulted in significant alleviation of OA progression in cartilage. Hence, our study may therefore introduce a new cell-free therapy based on exosomal miR-99 b-3p is considered a safe and effective alternative to stem cell therapies for OA.

However, when Exos are injected in vivo, they can be washed away easily due to the lack of a supporting matrix, which is the major challenge for using Exos in clinical applications [42,43]. Several studies have reported the controlled release of Exos from biomaterial systems [44,45]. Ideally, these systems should be deliverable in a minimally invasive manner and enhance vesicle retention in situ to facilitate Exos-induced cartilage formation.

HMPs have a number of unique properties compared to solid gel, that make them attractive for biomedical applications, and they have been widely used in biomedical research for cartilage repair, drug delivery and cell-based therapy [35,46,47]. First, their small size enables injection through small needles and catheters and inhalation of particles, which is advantageous for minimally invasive delivery of cells and biologics [48]. Second, HMPs can encapsulate different molecules or drugs and gradually release them by controlling their own degradation rate [47]. Third, properly sized HMPs provide good drug protection by minimizing clearance by blood vessels or lymphatics [46].

Repeated and regular injections tend to increase the incidence of adverse events, such as pain, joint bleeding and infection [49]. The degradation properties of intra-articular injected biomaterials are important for OA treatment. Good biodegradation activity is a necessary requirement for intra-articular drug carriers. We investigated the degradability and Exos release kinetics of HMPs@Exos to evaluate their use as an Exos carrier delivery system for long-term release. Hyaluronidase and H_2O_2 can act on the HMPs, leading to degradation of the HMPs and simultaneous release of the Exos. Both in vivo and in vitro experiment in this study showed a degradation rate of the HMPs approaching

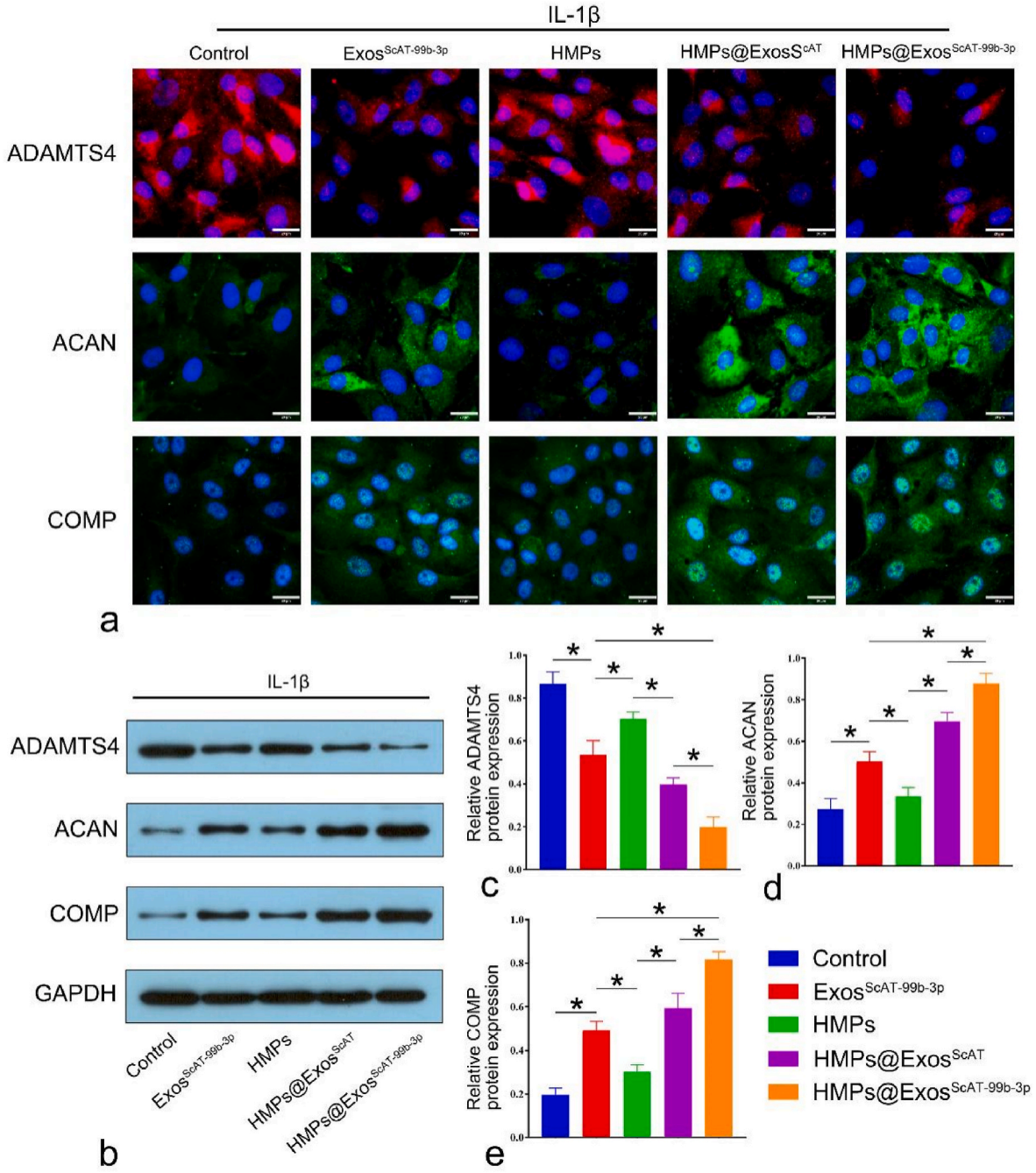

Fig. 9. Expression of ADAMTS4 and its substrates (ACAN, COMP) in intro. (a) Immunofluorescence analysis of ADAMTS4, ACAN, COMP in IL-1β induced chondrocytes on day 14. Scale bar = 20 μm. (b ~ e) ADAMTS4, ACAN, COMP expression levels were measured by western blotting on day 14. *$p < 0.05$.

nearly 28 days and predicted a slow release of Exos up to 28 days, which is very beneficial for long-term cartilage repair.

At present, there are several methods to prepare HMPs, including emulsions, microfluidics, and electrospray methods [50]. The microfluidic technique has obvious advantages in forming HMPs with controllable particle sizes and monodisperse particle sizes by adjusting the channel geometry and input flow rate. In this study, we used a microfluidic technique to prepare HMPs by Michael addition reaction with a uniform size and diameter of approximately 120 μm, which allowed the HMPs to smoothly pass through the syringe needle without resistance during injection. Our animal experiments confirmed that the HMPs prepared by microfluidic technology have good injectability, biocompatible, and the encapsulated Exos are well protected, facilitating maximal efficacy.

The current research existed several shortcomings. To begin with, the sample size of adipose tissue used for sequencing is relatively inadequate. Due to the fact that the participants are elderly individuals who may suffer from underlying chronic diseases, a significant level of heterogeneity may exist, leading to potential deviation in the sequencing outcomes. Secondly, the sequencing outcomes contain a substantial number of differentially expressed miRNAs. While miR-99 b-3p exhibits significant expression variations, it is just one of the different miRNAs. Other miRNAs might also have an impact on the results of chondrocytes metabolism. This study did not specifically investigate the roles of each individual miRNA. Thirdly, there has not been an in-depth investigation into the specific mechanism of action of miR-99 b-3p and its potential signaling pathways. Fourthly, the combination of HMPs, Exos and miRNA results in a complex system, and the reparative effect

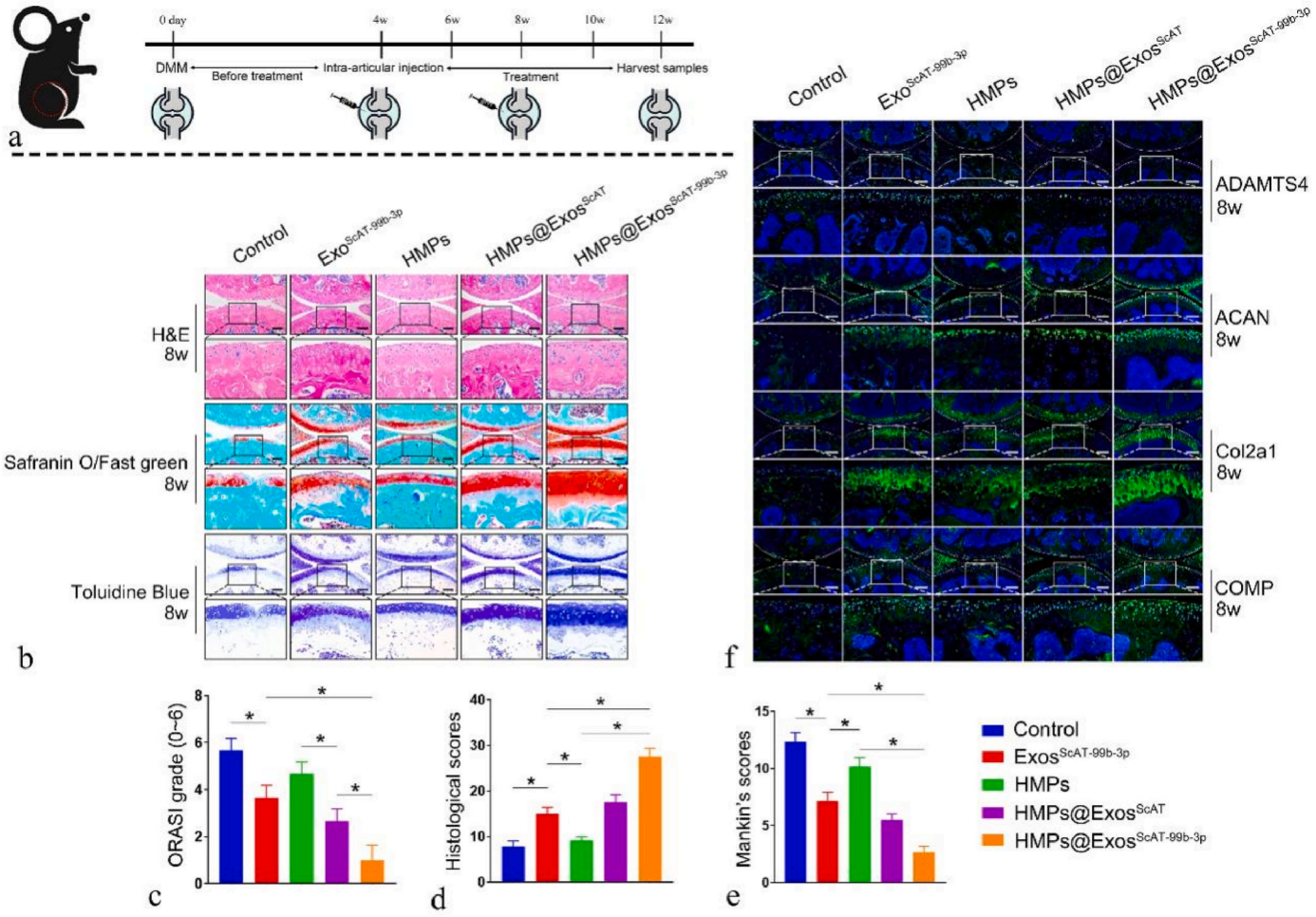

Fig. 10. In Vivo Therapeutic Effect of Osteoarthritis. (a) A flow diagram showing the time of intra-articular injection. (b) H&E, Safranin O/fast green, Toluidine Blue staining of mice knee joints on 8th week. Scale bar = 200 μm. (c) OARSI grade of the knee joints of DMM mice on 8th week. (d) Histological scores of the knee joints of DMM mice on 8th week. (E) Mankin's scores of the knee joints of DMM mice on 8th week. (f) Immunofluorescence analysis of ADAMTS4, ACAN, COMP and Col2a1 in knee joints of DMM mice on 8th week. Scale bar = 200 μm. Scale bar = 200 μm *$p < 0.05$. (For interpretation of the references to color in this figure legend, the reader is referred to the Web version of this article.)

on cartilage might not solely rely on miRNA as a single factor. In future research, we will further investigate the potential mechanisms involved.

5. Conclusion

In the present investigation, we have documented that $Exos^{IPFP}$ demonstrates a superior efficacy compared to $Exos^{ScAT}$ in addressing certain aspects of osteoarthritis (OA). Our findings from small RNA sequencing indicate a potential involvement of miR-99 b-3p in enhancing the ECM integrity. Utilizing various databases, ADAMTS4 has been identified as a potential target gene for miR-99 b-3p. Overexpression of miR-99 b-3p in Exos leads to the inhibition of ADAMTS4 expression, which subsequently enhances the expression of ECM components and improves the therapeutic efficacy against OA. In clinical applications, $Exos^{ScAT-99b-3p}$ (upregulation of miR-99 b-3p in $Exos^{ScAT}$) exhibit superior effectiveness to $Exos^{IPFP}$ for OA treatment, making it a promising approach for OA treatment. Moreover, considering the abundant resource of ScAT and the limited availability of IPFP, ScAT harvested through liposuction could be genetically engineered to yield Exos for OA treatment.

Furthermore, in order to address the issue of the short in vivo half-life of Exos, we performed microfluidic technology to fabricate HMPs capable of encapsulating Exos. The HMPs exhibited favorable characteristics such as extended Exos retention, enhanced biocompatibility, and facilitated ECM synthesis in chondrocytes. In murine models of osteoarthritis (OA), the $HMPs@Exos^{ScAT-99b-3p}$ showed gradually degradation, sustained release of $Exos^{ScAT-99b-3p}$ which exerted long-term inhibitory effects on ECM degradation while promoting the repair of damaged cartilage in OA. Collectively, the encapsulation of Exos in HMPs provides an injectable sustained local drug release system, which could potentially enhance the efficacy of Exos and hold potential as future therapeutic strategies.

Ethics approval and consent to participate

All experimental protocols with regard to the use of animals were approved by the Institutional Animal Care Committee of Nanjing First Hospital. All animal experiments were performed in accordance with the guidelines of decreasing the amount of suffering, pain, and discomfort of the experimental animals. Human clinical samples were obtained from patients who underwent total knee arthroplasties after informed consent and approval from the Ethics Committee of Nanjing First Hospital (Nanjing, China). All patients provided written informed consent prior to their inclusion within the study.

Consent for publication

All authors gave their consent for publication.

Availability of data and materials

The datasets used or analyzed during the current study are available from the corresponding author on reasonable request.

Credit author statement

Jianchao Gui: Conceptualization, Methodology, Funding acquisition, Writing - Review & Editing, Zhaowei Yin: Validation, Investigation, Resources, Writing - Original Draft, Chaoren Qin and Yan Feng: Data Curation, Formal analysis, Shaowei Pan and Chen shi: Visualization, Formal analysis, Fu Guan and Jing Zhang: Resources, Investigation, Formal analysis, Visualization, Ziyi Yu: Conceptualization, Bin Liang: Supervision, All authors reviewed the manuscript.

Declaration of competing interest

The authors declare that they have no known competing financial interests or personal relationships that could have appeared to influence the work reported in this paper.

Data availability

Data will be made available on request.

Acknowledgements

This work was supported by National Key Research and Development Program of China (2021YFC2104300) and the National Natural Science Foundation of China (22278214, 52273207). The authors also would like to acknowledge the support of Natural Science Foundation of Jiangsu Province (BK20221314) and State Key Laboratory of Materials-Oriented Chemical Engineering (SKL-MCE-22A06)

Appendix A. Supplementary data

Supplementary data to this article can be found online at https://doi.org/10.1016/j.mtbio.2023.100813.

References

[1] J. Wen, H. Li, H. Dai, S. Hua, X. Long, H. Li, S. Ivanovski, C. Xu, Intra-articular nanoparticles based therapies for osteoarthritis and rheumatoid arthritis management, Mater Today Bio 19 (2023), 100597, https://doi.org/10.1016/j.mtbio.2023.100597.

[2] X. Du, Z.-Y. Liu, X.-X. Tao, Y.-L. Mei, D.-Q. Zhou, K. Cheng, S.-L. Gao, H.-Y. Shi, C. Song, X.-M. Zhang, Research Progress on the Pathogenesis of Knee Osteoarthritis, Orthop Surg, 2023, https://doi.org/10.1111/os.13809.

[3] W. Xie, S. Qi, L. Dou, L. Wang, X. Wang, R. Bi, N. Li, Y. Zhang, Achyranthoside D attenuates chondrocyte loss and inflammation in osteoarthritis via targeted regulation of Wnt3a, Phytomedicine 111 (2023), 154663, https://doi.org/10.1016/j.phymed.2023.154663.

[4] T. Zhou, J. Ran, P. Xu, L. Shen, Y. He, J. Ye, L. Wu, C. Gao, A hyaluronic acid/platelet-rich plasma hydrogel containing MnO2 nanozymes efficiently alleviates osteoarthritis in vivo, Carbohydr. Polym. 292 (2022), 119667, https://doi.org/10.1016/j.carbpol.2022.119667.

[5] H. Yang, Z. Wang, L. Wang, Y. Li, J. Guo, X. Yang, J. Zhao, K. Rong, P. Zhang, B. Ye, K. Zhang, H. Ma, Scutellarin ameliorates osteoarthritis by protecting chondrocytes and subchondral bone microstructure by inactivating NF-κB/MAPK signal transduction, Biomed. Pharmacother. 155 (2022), 113781, https://doi.org/10.1016/j.biopha.2022.113781.

[6] S. Li, J. Yang, J. Sun, M. Chen, Adipose-derived mesenchymal stem cells alleviate hypertrophic scar by inhibiting bioactivity and inducing apoptosis in hypertrophic scar fibroblasts, Cells 11 (2022) 4024, https://doi.org/10.3390/cells11244024.

[7] S. Liu, R. Li, K. Dou, K. Li, Q. Zhou, Q. Fu, Injectable thermo-sensitive hydrogel containing ADSC-derived exosomes for the treatment of cavernous nerve injury, Carbohydr. Polym. 300 (2023), 120226, https://doi.org/10.1016/j.carbpol.2022.120226.

[8] T. Jiang, S. Liu, Z. Wu, Q. Li, S. Ren, J. Chen, X. Xu, C. Wang, C. Lu, X. Yang, Z. Chen, ADSC-exo@MMP-PEG smart hydrogel promotes diabetic wound healing by optimizing cellular functions and relieving oxidative stress, Materials Today Bio 16 (2022), 100365, https://doi.org/10.1016/j.mtbio.2022.100365.

[9] C.-F. Chen, C.-C. Hu, C.-T. Wu, H.-T.H. Wu, C.-S. Chang, Y.-P. Hung, C.-C. Tsai, Y. Chang, Treatment of knee osteoarthritis with intra-articular injection of allogeneic adipose-derived stem cells (ADSCs) ELIXCYTE®: a phase I/II, randomized, active-control, single-blind, multiple-center clinical trial, Stem Cell Res. Ther. 12 (2021) 1–12, https://doi.org/10.1186/s13287-021-02631-z.

[10] L. Rochette, L. Mazini, G. Malka, M. Zeller, Y. Cottin, C. Vergely, The crosstalk of adipose-derived stem cells (ADSC), oxidative stress, and inflammation in protective and adaptive responses, Indian J. Manag. Sci. 21 (2020) 9262, https://doi.org/10.3390/ijms21239262.

[11] N. Billon, C. Dani, Developmental origins of the adipocyte lineage: new insights from genetics and genomics studies, Stem Cell Rev and Rep 8 (2012) 55–66, https://doi.org/10.1007/s12015-011-9242-x.

[12] N. Lanthier, I.A. Leclercq, Adipose tissues as endocrine target organs, Best Pract. Res. Clin. Gastroenterol. 28 (2014) 545–558, https://doi.org/10.1016/j.bpg.2014.07.002.

[13] T. Mochizuki, T. Muneta, Y. Sakaguchi, A. Nimura, A. Yokoyama, H. Koga, I. Sekiya, Higher chondrogenic potential of fibrous synovium– and adipose synovium–derived cells compared with subcutaneous fat–derived cells: distinguishing properties of mesenchymal stem cells in humans, Arthritis Rheum. 54 (2006) 843–853, https://doi.org/10.1002/art.21651.

[14] M.M. Ibrahim, Subcutaneous and visceral adipose tissue: structural and functional differences, Obes. Rev. 11 (2010) 11–18, https://doi.org/10.1111/j.1467-789X.2009.00623.x.

[15] M.Q. Wickham, G.R. Erickson, J.M. Gimble, T.P. Vail, F. Guilak, Multipotent stromal cells derived from the infrapatellar fat pad of the knee, Clin. Orthop. Relat. Res. 412 (2003) 196–212, https://doi.org/10.1097/01.blo.0000072467.53786.ca.

[16] V. Lu, M. Tennyson, J. Zhang, W. Khan, Mesenchymal stem cell-derived extracellular vesicles in tendon and ligament repair—a systematic Review of in vivo studies, Cells 10 (2021) 2553, https://doi.org/10.3390/cells10102553.

[17] H. Sun, R.E. Pratt, C.P. Hodgkinson, V.J. Dzau, Sequential paracrine mechanisms are necessary for the therapeutic benefits of stem cell therapy, Am. J. Physiol. Cell Physiol. 319 (2020), https://doi.org/10.1152/ajpcell.00516.2019. C1141–C1150.

[18] J. Ma, L. Yong, P. Lei, H. Li, Y. Fang, L. Wang, H. Chen, Q. Zhou, W. Wu, L. Jin, D. Sun, X. Zhang, Advances in microRNA from adipose-derived mesenchymal stem cell-derived exosome: focusing on wound healing, J. Mater. Chem. B 10 (2022) 9565–9577, https://doi.org/10.1039/D2TB01987F.

[19] X. Gui, H. Zhang, R. Zhang, Q. Li, W. Zhu, Z. Nie, J. Zhao, X. Cui, W. Hao, X. Wen, W. Shen, H. Song, Exosomes incorporated with black phosphorus quantum dots attenuate retinal angiogenesis via disrupting glucose metabolism, Mater Today Bio 19 (2023), 100602, https://doi.org/10.1016/j.mtbio.2023.100602.

[20] Y. Zhang, X. Wang, J. Chen, D. Qian, P. Gao, T. Qin, T. Jiang, J. Yi, T. Xu, Y. Huang, Q. Wang, Z. Zhou, T. Bao, X. Zhao, H. Liu, Z. Zheng, J. Fan, S. Zhao, Q. Li, G. Yin, Exosomes derived from platelet-rich plasma administration in site mediate cartilage protection in subtalar osteoarthritis, J. Nanobiotechnol. 20 (2022) 56, https://doi.org/10.1186/s12951-022-01245-8.

[21] Y. Liu, Y. Zeng, H.-B. Si, L. Tang, H.-Q. Xie, B. Shen, Exosomes derived from human urine–derived stem cells overexpressing miR-140-5p alleviate knee osteoarthritis through downregulation of VEGFA in a rat model, Am. J. Sports Med. 50 (2022) 1088–1105, https://doi.org/10.1177/03635465221073991.

[22] J. Lei, X. Jiang, W. Li, J. Ren, D. Wang, Z. Ji, Z. Wu, F. Cheng, Y. Cai, Z.-R. Yu, J.C. I. Belmonte, C. Li, G.-H. Liu, W. Zhang, J. Qu, S. Wang, Exosomes from antler stem cells alleviate mesenchymal stem cell senescence and osteoarthritis, Protein Cell 13 (2022) 220–226, https://doi.org/10.1007/s13238-021-00860-9.

[23] Y. Liang, X. Xu, X. Li, J. Xiong, B. Li, L. Duan, D. Wang, J. Xia, Chondrocyte-Targeted MicroRNA delivery by engineered exosomes toward a cell-free osteoarthritis therapy, ACS Appl. Mater. Interfaces 12 (2020) 36938–36947, https://doi.org/10.1021/acsami.0c10458.

[24] F. Li, Z. Xu, Z. Xie, X. Sun, C. Li, Y. Chen, J. Xu, G. Pi, Adipose mesenchymal stem cells-derived exosomes alleviate osteoarthritis by transporting microRNA -376c-3p and targeting the WNT-beta-catenin signaling axis, Apoptosis (2022), https://doi.org/10.1007/s10495-022-01787-0.

[25] Y. Chen, H. Huang, W. Zhong, L. Li, Y. Lu, H. Si, miR-140-5p protects cartilage progenitor/stem cells from fate changes in knee osteoarthritis, Int. Immunopharm. 114 (2023), 109576, https://doi.org/10.1016/j.intimp.2022.109576.

[26] D. Cai, J. Zhang, J. Yang, Q. Lv, C. Zhong, Overexpression of FTO alleviates osteoarthritis by regulating the processing of miR-515-5p and the TLR4/MyD88/NF-κB axis, Int. Immunopharm. 114 (2023), 109524, https://doi.org/10.1016/j.intimp.2022.109524.

[27] J. Wu, L. Kuang, C. Chen, J. Yang, W.-N. Zeng, T. Li, H. Chen, S. Huang, Z. Fu, J. Li, R. Liu, Z. Ni, L. Chen, L. Yang, miR-100-5p-abundant exosomes derived from infrapatellar fat pad MSCs protect articular cartilage and ameliorate gait abnormalities via inhibition of mTOR in osteoarthritis, Biomaterials 206 (2019) 87–100, https://doi.org/10.1016/j.biomaterials.2019.03.022.

[28] J. Garcia, K. Wright, S. Roberts, J.H. Kuiper, C. Mangham, J. Richardson, C. Mennan, Characterisation of synovial fluid and infrapatellar fat pad derived mesenchymal stromal cells: the influence of tissue source and inflammatory stimulus, Sci. Rep. 6 (2016), 24295, https://doi.org/10.1038/srep24295.

[29] I.R. Klein-Wieringa, M. Kloppenburg, Y.M. Bastiaansen-Jenniskens, E. Yusuf, J. C. Kwekkeboom, H. El-Bannoudi, R.G.H.H. Nelissen, A. Zuurmond, V. Stojanovic-Susulic, G.J.V.M. Van Osch, R.E.M. Toes, A. Ioan-Facsinay, The infrapatellar fat pad of patients with osteoarthritis has an inflammatory phenotype, Ann. Rheum. Dis. 70 (2011) 851–857, https://doi.org/10.1136/ard.2010.140046.

[30] A. Skubis-Sikora, B. Sikora, A. Witkowska, U. Mazurek, J. Gola, Osteogenesis of adipose-derived stem cells from patients with glucose metabolism disorders, Mol. Med. 26 (2020) 67, https://doi.org/10.1186/s10020-020-00192-0.

[31] N. Hu, Z. Cai, X. Jiang, C. Wang, T. Tang, T. Xu, H. Chen, X. Li, X. Du, W. Cui, Hypoxia-pretreated ADSC-derived exosome-embedded hydrogels promote angiogenesis and accelerate diabetic wound healing, Acta Biomater. 157 (2023) 175–186, https://doi.org/10.1016/j.actbio.2022.11.057.

[32] Q. Sun, W. Yin, X. Ru, C. Liu, B. Song, Z. Qian, Dual role of injectable curcumin-loaded microgels for efficient repair of osteoarthritic cartilage injury, Front. Bioeng. Biotechnol. 10 (2022), 994816, https://doi.org/10.3389/fbioe.2022.994816.

[33] W. Xiong, Q. Lan, X. Liang, J. Zhao, H. Huang, Y. Zhan, Z. Qin, X. Jiang, L. Zheng, Cartilage-targeting poly(ethylene glycol) (PEG)-formononetin (FMN) nanodrug for the treatment of osteoarthritis, J. Nanobiotechnol. 19 (2021) 197, https://doi.org/10.1186/s12951-021-00945-x.

[34] Y. Wang, L. Chen, D.-Y. Ren, Z.-X. Feng, L.-Y. Zhang, Y.-F. Zhong, M.-Y. Jin, F.-W. Xu, C.-Y. Feng, Y.-Z. Du, W.-Q. Tan, Mussel-inspired collagen-hyaluronic acid composite scaffold with excellent antioxidant properties and sustained release of a growth factor for enhancing diabetic wound healing, Mater Today Bio 15 (2022), 100320, https://doi.org/10.1016/j.mtbio.2022.100320.

[35] H. Yu, C. Huang, X. Kong, J. Ma, P. Ren, J. Chen, X. Zhang, H. Luo, G. Chen, Nanoarchitectonics of cartilage-targeting hydrogel microspheres with reactive oxygen species responsiveness for the repair of osteoarthritis, ACS Appl. Mater. Interfaces 14 (2022) 40711–40723, https://doi.org/10.1021/acsami.2c12703.

[36] J. Zhang, H. Yong, S. A, Q. Xu, Y. Miao, J. Lyu, Y. Gao, M. Zeng, D. Zhou, Z. Yu, H. Tai, W. Wang, Structural Design of robust and biocompatible photonic hydrogels from an in situ cross-linked hyperbranched polymer system, Chem. Mater. 30 (2018) 6091–6098, https://doi.org/10.1021/acs.chemmater.8b02542.

[37] H. Xu, M. Sun, C. Wang, K. Xia, S. Xiao, Y. Wang, L. Ying, C. Yu, Q. Yang, Y. He, A. Liu, L. Chen, Growth differentiation factor-5–gelatin methacryloyl injectable microspheres laden with adipose-derived stem cells for repair of disc degeneration, Biofabrication 13 (2020), 015010, https://doi.org/10.1088/1758-5090/abc4d3.

[38] M.L. Tiku, H.E. Sabaawy, Cartilage regeneration for treatment of osteoarthritis: a paradigm for nonsurgical intervention, Therapeutic Advances in Musculoskeletal 7 (2015) 76–87, https://doi.org/10.1177/1759720X15576866.

[39] P. Meng, F. Zhang, Y. Zhang, H. Wei, S. Tan, X. Guo, S. Wang, Y. Yu, ADAMTS4 and ADAMTS5 may be considered as new molecular therapeutic targets for cartilage damages with Kashin-Beck Disease, Med. Hypotheses 135 (2020), 109440, https://doi.org/10.1016/j.mehy.2019.109440.

[40] P. Verma, K. Dalal, ADAMTS-4 and ADAMTS-5: key enzymes in osteoarthritis, J. Cell. Biochem. 112 (2011) 3507–3514, https://doi.org/10.1002/jcb.23298.

[41] M.D. Tortorella, A.-M. Malfait, C. Deccico, E. Arner, The role of ADAM-TS4 (aggrecanase-1) and ADAM-TS5 (aggrecanase-2) in a model of cartilage degradation, Osteoarthritis Cartilage 9 (2001) 539–552, https://doi.org/10.1053/joca.2001.0427.

[42] C. Han, J. Zhou, B. Liu, C. Liang, X. Pan, Y. Zhang, Y. Zhang, Y. Wang, L. Shao, B. Zhu, J. Wang, Q. Yin, X.-Y. Yu, Y. Li, Delivery of miR-675 by stem cell-derived exosomes encapsulated in silk fibroin hydrogel prevents aging-induced vascular dysfunction in mouse hindlimb, Mater. Sci. Eng. C 99 (2019) 322–332, https://doi.org/10.1016/j.msec.2019.01.122.

[43] Y. Takahashi, M. Nishikawa, H. Shinotsuka, Y. Matsui, S. Ohara, T. Imai, Y. Takakura, Visualization and in vivo tracking of the exosomes of murine melanoma B16-BL6 cells in mice after intravenous injection, J. Biotechnol. 165 (2013) 77–84, https://doi.org/10.1016/j.jbiotec.2013.03.013.

[44] N. Nikravesh, O.G. Davies, I. Azoidis, R.J.A. Moakes, L. Marani, M. Turner, C. J. Kearney, N.M. Eisenstein, L.M. Grover, S.C. Cox, Physical structuring of injectable polymeric systems to controllably deliver nanosized extracellular vesicles, Adv. Healthcare Mater. 8 (2019), 1801604, https://doi.org/10.1002/adhm.201801604.

[45] E.A. Mol, Z. Lei, M.T. Roefs, M.H. Bakker, M. Goumans, P.A. Doevendans, P.Y. W. Dankers, P. Vader, J.P.G. Sluijter, Injectable supramolecular ureidopyrimidinone hydrogels provide sustained release of extracellular vesicle therapeutics, Adv. Healthcare Mater. 8 (2019), 1900847, https://doi.org/10.1002/adhm.201900847.

[46] J. Lin, L. Chen, J. Yang, X. Li, J. Wang, Y. Zhu, X. Xu, W. Cui, Injectable double positively charged hydrogel microspheres for targeting-penetration-phagocytosis, Small 18 (2022), 2202156, https://doi.org/10.1002/smll.202202156.

[47] Y. Han, J. Yang, W. Zhao, H. Wang, Y. Sun, Y. Chen, J. Luo, L. Deng, X. Xu, W. Cui, H. Zhang, Biomimetic injectable hydrogel microspheres with enhanced lubrication and controllable drug release for the treatment of osteoarthritis, Bioact. Mater. 6 (2021) 3596–3607, https://doi.org/10.1016/j.bioactmat.2021.03.022.

[48] Y.-J. Seong, G. Lin, B.J. Kim, H.-E. Kim, S. Kim, S.-H. Jeong, Hyaluronic acid-based hybrid hydrogel microspheres with enhanced structural stability and high injectability, ACS Omega 4 (2019) 13834–13844, https://doi.org/10.1021/acsomega.9b01475.

[49] N. Gerwin, C. Hops, A. Lucke, Intraarticular drug delivery in osteoarthritis☆, Adv. Drug Deliv. Rev. 58 (2006) 226–242, https://doi.org/10.1016/j.addr.2006.01.018.

[50] A.C. Daly, L. Riley, T. Segura, J.A. Burdick, Hydrogel microparticles for biomedical applications, Nat. Rev. Mater. 5 (2020) 20–43, https://doi.org/10.1038/s41578-019-0148-6.